RSC Advances

PAPER

View Article Online
View Journal | View Issue

Cite this: *RSC Adv.*, 2026, **16**, 10798

Physics-encoded machine learning for performance and emission prediction of nickel ferrite nanocatalyst and hydrogen-enriched biodiesel in diesel engines

Nguyen Van Minh,[ab] Ravikumar Jayabal,[c] Lionus Leo G M,[d] Sekar S,[e] Karthikeyan L,[f] Robinson Joseph,[g] Jothilakshmi P[h] and Rajkumar Sivanraju *[i]

This work examined the combined effects of waste cooking oil biodiesel (WCOB), $NiFe_2O_4$ nanocatalysts, and hydrogen (H_2) enrichment on in-cylinder processes, engine performance, and emissions of a diesel engine. To accurately represent the physical processes and to derive thermodynamically consistent predictions, a physics-encoded multi-task machine learning (PE-MTMML) model was developed. Tests were carried out on a single-cylinder, four-stroke diesel engine at 1500 rpm. The engine was operated on blends of diesel, WCOB, and $NiFe_2O_4$ (50–150 ppm) with the addition of H_2 at 5 LPM. The analysis of combustion was done based on the measurement of in-cylinder pressure with respect to the crank angle from which peak pressure and heat release rate (HRR) were derived using a single-zone model. Performance parameters were obtained at various loads through the full load range. The PE-MTMML model incorporated not only the thermodynamic reciprocity but also catalytic oxidation trends and root-sum-square (RSS) uncertainty constraints. At full load, the $NiFe_2O_4$ nanoparticles improved catalytic oxidation and premixed combustion, thus, the peak pressure rose by 7.8% at most, and HRR by 14% compared to diesel. The ensemble of WCOB + $NiFe_2O_4$ 150 ppm + H_2 led to an increase in brake thermal efficiency (BTE) of 29.2% and a decrease in brake-specific energy consumption (BSEC) of 22.3% in comparison with diesel. Inspection of emissions revealed that the smoke opacity was lessened by 10.9%, carbon monoxide (CO) by 20%, and hydrocarbons (HC) by 25%, while nitrogen oxides (NO_x) were elevated by 7.5% relative to diesel. The PE-MTMML model had excellent prediction capabilities (mean R^2 = 0.9993) and at the same time adhered to thermodynamic constraints. The synergistic effect of $NiFe_2O_4$ nanocatalysis and H_2 enrichment makes WCOB both a high-efficiency and a low-pollution fuel. By allowing for optimization with minimal experimental input, the PE-MTMML scheme acts as a trustworthy digital twin, supporting circular-economy goals and the transition to sustainable, carbon-neutral diesel engines.

Received 3rd December 2025
Accepted 17th February 2026

DOI: 10.1039/d5ra09336h

rsc.li/rsc-advances

1 Introduction

With the rapid depletion of fossil fuel reserves and escalating environmental concerns, the global transition toward renewable and low-carbon fuels has accelerated.[1] In this context, biodiesel, a renewable fuel derived from biological lipids such as vegetable oils, animal fats, and waste oil, has been accepted as a feasible substitute for petroleum diesel due to its biodegradability, lower carbon footprint, and compatibility with existing engines.[2] Biodiesel possess superior characteristics compared to petroleum diesel, including higher oxygen content, enhanced lubricity, and reduced CO and smoke emissions.[3] Nevertheless, some obstacles *i.e.* higher viscosity, lower volatility, and reduced calorific value, which can negatively influence atomization and combustion efficiency, thereby resulting in increase of NO_x emissions, are still responsible for its limited use.[4]

[a]*Institute of Research and Development, Duy Tan University, Da Nang 550000, Vietnam*
[b]*School of Engineering & Technology, Duy Tan University, Da Nang 550000, Vietnam*
[c]*Department of Mechanical Engineering, Academy of Maritime Education and Training, AMET University, Kanathur, Chennai, Tamil Nadu, India*
[d]*Department of Mechanical Engineering, St. Joseph's College of Engineering, Chennai, Tamil Nadu, India*
[e]*Department of Mechanical Engineering, Rajalakshmi Engineering College, Chennai, Tamil Nadu, India*
[f]*Department of Mechanical Engineering, Panimalar Engineering College, Chennai-600123, India*
[g]*School of Business, Horizon University College, Ajman, United Arab Emirates*
[h]*Department of Electronics and Communication Engineering, Amrita School of Engineering, Amrita Vishwa Vidyapeetham, Chennai, Tamil Nadu, India*
[i]*Department of Mechanical Engineering, Faculty of Manufacturing, Institute of Technology, Hawassa University, Ethiopia. E-mail: rajkumar@hu.edu.et*

The problem of how to improve combustion characteristics and the emission performance of systems using biodiesel as a fuel remains to be solved.[5] Different studies have investigated the use of biodiesel in diesel engines to improve engine performance and reduce pollutant emissions.[6–8] Among various biofuels, waste cooking oil biodiesel (WCOB) has been highly favored because of its cheapness, easy accessibility, and the potential of waste valorization.[2,9–12] Some experimental studies present that WCOB blends could lead to an increase of BTE by 10% and a decrease of smoke opacity by 30% compared to that of a conventional diesel setup.[5–8] Also, palm oil methyl ester [13–15] and Jatropha-based biodiesel[16–19] have been reported to emit less CO and HC, but almost NO_x is a little higher, which is attributed to the oxygen-rich combustion process.[14] Some of the most recent discoveries also show that the biodiesel made from the used frying oil can be used as renewable fuel for up to 20% without a negative effect on the mustards or the stability of the engine.[20] Moreover, a microemulsified biodiesel blend has been associated with easier atomization and an increased heat release rate, thus resulting in better combustion stability.[21] These works of research, in concert, provide positive proof of the benefits of biodiesel in terms of environment and operation, and at the same time, they indicate the requirement to create strategies for combustion to counteract the performance-related drawbacks.

To mitigate these challenges, current research is focused on the utilization of nanomaterials as fuel-borne catalysts.[22–28] Nanoparticles have immense surface-to-volume ratios, catalytic reactivity, and thermal conductivity.[29] As a result, they are very effective in combustion kinetics and emission characteristics.[18,30–37] Nanoparticles in a biodiesel medium may act as oxygen buffers,[38–40] thus allowing the carbonaceous species to be completely oxidized and, therefore, the ignition delay to be lowered.[41–43] Previous research indicates that the addition of cerium oxide (CeO_2) nanoparticles to the biodiesel significantly reduced CO and unburned HC emissions by more than 40%.[44–47] By mixing Al_2O_3 nanoparticles with biodiesel, BTE was raised by 9% and smoke emissions were reduced.[24,48–51] In similar, TiO_2 nanocatalysts in WCOB elevated the heat release rate and lowered particulate matter.[50–53] Out of these, the research on spinel ferrite nanomaterials, primarily $NiFe_2O_4$, has been intensified due to their high redox activity, magnetic properties, and thermal stability.[29,54–58] $NiFe_2O_4$ nanoparticles can catalyze oxidation reactions, generate radicals, and even electron transfer, thereby can quickly help in-cylinder combustion processes.[59,60] Additionally, they can be made cheaply from industrial waste, thus being in line with the circular economy and sustainable materials reuse concepts.[54]

Alongside nanotechnology, the H_2 enrichment of biodiesel-fueled engines has become one of the effective ways to attain cleaner and more efficient combustion. H_2 has been noted to have a very high flame speed, a very wide flammability range, and to produce zero-carbon combustion.[61–64] In the case of H_2 being used as a supplementary fuel, it supports premixed flame propagation, raises thermal efficiency, and cuts down CO and HC emissions.[56,65–68] Similarly, experimental works have been able to demonstrate that H_2 fumigation in biodiesel-operated diesel engines can have a positive influence on BTE up to 15% and the CO emissions can be reduced by 35%.[69] In addition to that, H_2 superior diffusivity allows for a more uniform air-fuel mixing that results in quicker oxidation of the fuel-rich zones and less soot production.[70] Though, the H_2 addition may raise the NO_x formation because of its very high adiabatic flame temperature and, therefore, the NO_x must be controlled by the injection of optimized timing or exhaust gas recirculation (EGR).[64]

Recent studies have moved toward the development of tri-fuel systems that combine biodiesel, nanoparticles, and H_2 in a synergistic manner, thus, representing a compelling avenue for high-efficiency and low-emission combustion as demonstrated by recent experimental investigations[64,71–73] and machine learning simulations.[74–76] In such setups, biodiesel is a source of renewable carbon and oxygen, H_2 as a source of combustion speed and thermal efficiency, and nanoparticles as oxidation catalysts in the cylinder. In another study, the authors found that adding CeO_2 nanoparticles to the H_2-enriched biodiesel resulted in an 18% increase in BTE and a 45% reduction in smoke opacity as compared to diesel.[77] Likewise, the presence of Al_2O_3 nanoparticles in the H_2-assisted biodiesel led to the improvement in the atomization process and reduction of the CO emission by 38%.[78] The TiO_2 nanoparticles in H_2-fumigated WCOB effectuated rapid and clean combustion.[79] Lately, the use of ferrite nanocatalysts has raised the oxidation stability and alleviated the unburned hydrocarbons in the H_2-assisted biodiesel engine.[80] In summary, the major effects of nanoparticles are catalytic oxidation and oxygen buffering, and thus, tri-fuel strategies have been demonstrated to produce these synergistic effects. H_2 is responsible for quick flame propagation and clean oxidation, and biodiesel, being a renewable source, is the energy carrier. However, the constraints of $NiFe_2O_4$ nanocatalysts in H_2-assisted biodiesel engines have not been sufficiently addressed and could be a potential area for further research.

Also, based on the reported research, biodiesel offers a lower environmental impact,[1,2] while nanoparticles enhance oxidation and heat transfer.[18,34–37] Furthermore, H_2 enrichment significantly improves flame propagation and thermal efficiency.[62,70,81–83] However, in the cited references, these factors have been primarily investigated separately or in binary combinations. Only a limited number of studies have combined these three elements, biodiesel, nanocatalyst, and H_2 into a unified tri-fuel concept, particularly utilizing waste-derived feedstocks and transition-metal ferrite catalysts.[81,83–86]

Consequently, this work introduces a novel tri-fuel strategy to investigate the synergistic effects of WCOB, $NiFe_2O_4$ nanocatalysts, and H_2 enrichment on the combustion, performance, and emission characteristics of a single-cylinder diesel engine. The primary goal of the work is to enhance the qualities of biodiesel that are naturally disadvantaged in terms of atomization, thermal efficiency, and carbon-based emissions by using catalytic oxidation and reactive fuel enhancement. Furthermore, a key objective of this work is to develop a physics-encoded multi-task machine learning (PE-MTMML) framework capable of forecasting engine behavior with

thermodynamic consistency, thereby creating a trustworthy digital twin for optimization and extrapolation beyond the experimental region.

This work introduces a novel tri-fuel strategy combining waste cooking oil biodiesel, $NiFe_2O_4$ nanocatalysts, and H_2 enrichment a configuration not previously investigated. A primary innovation is the development of a physics-encoded multi-task machine learning (PE-MTMML) framework,[87–91] implemented using PyTorch 2.4 (ref. 92) that integrates thermodynamic and emission-formation principles for accurate, physically consistent prediction. This digital twin facilitates the optimization of fuel blends and H_2 flow rates with minimal experimental input, thereby advancing sustainability-driven innovations for carbon-neutral engine technologies.

2 Materials and methods

2.1 Raw oil collection and biodiesel production

Waste cooking oil was collected from restaurants and institutional kitchens in the local area. Collected oil was filtered to remove food particles, heated to 105 °C for 4–6 h to remove moisture, and allowed to settle. Residual solids were removed by centrifugation at 4000 rpm for 15 min. The cleaned oil was characterized by acid value and free fatty acids (FFA) per ASTM D664. Oils with FFA > 2 wt% were pretreated *via* acid esterification.

WCOB production used a two-stage acid esterification-base transesterification to maximize conversion.[93] For acid pretreatment, methanol and concentrated sulfuric acid (1 wt% of oil) were reacted with oil at a 6 : 1 methanol:oil molar ratio, 55 °C, 60 min under stirring. After phase separation and glycerol removal, the oil proceeded to base transesterification using methanol (6 : 1 molar ratio) and KOH (1 wt% of oil) at 60 °C for 90 min. The mixture was allowed to settle for 8 h to separate glycerol. The upper methyl ester layer was washed with warm distilled water until neutral pH and dried at 105 °C for 1 h. Biodiesel yield and conversion were estimated gravimetrically; typical conversion exceeded 95%.

2.2 Test fuel preparation

For the experimental study, WCOB served as the base fuel, and $NiFe_2O_4$ nanoparticles were introduced as combustion-enhancing nanocatalysts. The $NiFe_2O_4$ nanoparticles (average particle size 25–30 nm, purity >99.5%) were first oven-dried at 105 °C for 2 h to remove moisture. Measured quantities corresponding to 50, 100, and 150 ppm concentrations were accurately weighed and dispersed in preheated WCOB. The dispersion steps consisted of magnetic stirring at 60 °C for 15 min, followed by probe ultrasonication at 20 kHz and 400 W for 30 min. This was done to get a homogeneous suspension and to minimize agglomeration. To prevent the settling of nanoparticles during prolonged storage, a small amount of nonionic surfactant Span-80 (0.1 wt%) was used. The prepared nanocarbon-based fuel (NCB) blends were named as WCOB + $NiFe_2O_4$ (50 ppm), WCOB + $NiFe_2O_4$ (100 ppm), and WCOB + $NiFe_2O_4$ (150 ppm). The stability of such blends was ascertained by UV-Vis spectrophotometry and zeta potential measurement, with the latter giving values between −35 mV and −43 mV, thus indicating dispersion stability. For tri-fuel operation, H_2 gas of 99.99% purity was delivered from a high-pressure cylinder and mixed with the intake air through a calibrated rotameter-controlled system at a fixed flow rate of 5 LPM. This hybrid configuration of WCOB, $NiFe_2O_4$ nanocatalyst, and H_2 enrichment were designed to achieve improved atomization, catalytic oxidation, and H_2-assisted flame propagation resulting in higher thermal efficiency and lower carbon-based emissions in a stationary diesel engine. Table 1 shows the test fuel properties.

2.3 Experimental setup and facility

The study aimed to demonstrate the usage of WCOB and nanoparticle-enriched fuel blends for a H_2-assisted diesel engine. A single-cylinder, four-stroke, water-cooled, direct injection diesel engine was used to assess the performance, combustion, and emission characteristics of the WCOB and its $NiFe_2O_4$ nanoparticle-enriched blend under H_2-assisted combustion. The engine's simple structure, sturdy construction, and easy-to-setup instrumentation proved to be convenient for a reproducible experimental study. An eddy-current dynamometer varied the loads from 0% to 100%, while the engine speed was kept at 1500 rpm. All the tests were conducted under steady-state conditions to allow a systematic assessment of combustion, performance, and emission characteristics for diesel, WCOB, and H_2-assisted nanofuel blends (Fig. 1). The in-cylinder pressure measurement was done with an AVL GU22C piezoelectric transducer that was mounted flush with the cylinder head. Moreover, a high-resolution crank-angle encoder was used to synchronize data acquisition at 1 °CA intervals. The average pressure data (100 cycles) served to calculate heat release rate (HRR) and rate of pressure rise through a LabVIEW-based single-zone thermodynamic model with variables. From

Table 1 Test fuel properties

Property	ASTM method	Diesel	WCOB	WCOB + $NiFe_2O_4$ 50 ppm	WCOB + $NiFe_2O_4$ 100 ppm	WCOB + $NiFe_2O_4$ 150 ppm
Density@15 °C (kg m^{-3})	D1298	830	880	878	876	874
Kinematic viscosity@40 °C (cSt)	D445	2.65	4.8	4.5	4.2	3.9
Flash point (°C)	D93	62	162	155	150	145
Calorific value (MJ kg^{-1})	D240	43.1	39.6	39.9	40.3	40.8
Cetane number	D613	48	57	56	55	54
Oxygen content (wt%)	D5622	0	10.8	10.6	10.4	10.2
Carbon content (wt%)	D5291	86.3	77.2	77.4	77.6	77.8

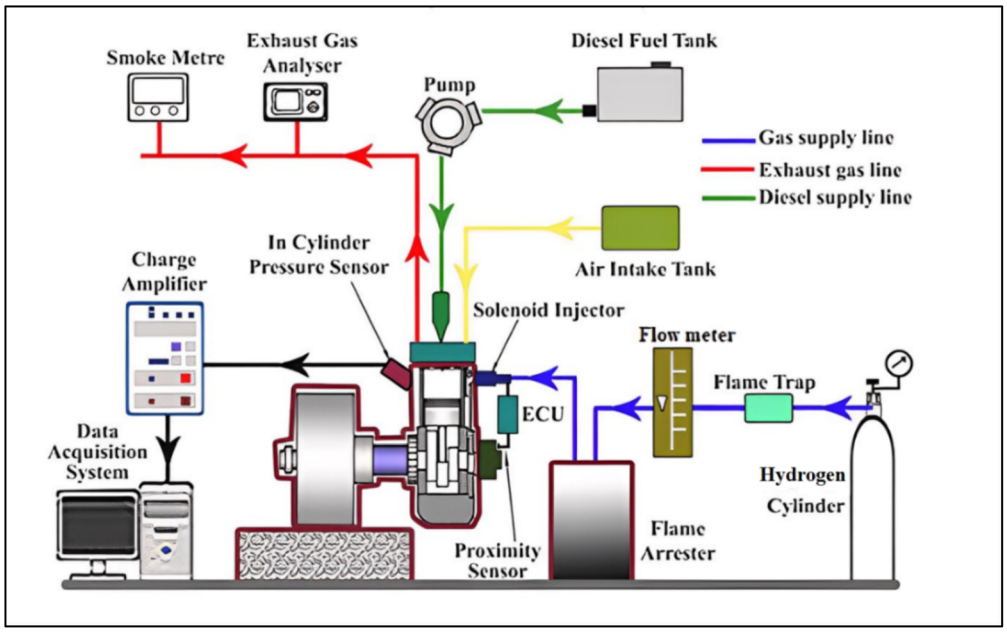

Fig. 1 Experimental layout.

this thermodynamic analysis, key combustion parameters were derived, including the start of combustion (SOC) and the CA50 (the crank angle position where 50% of the fuel mass fraction is burned), which represents the centroid of the heat release process.[94,95]

High-purity hydrogen gas (99.99%) was delivered to the intake manifold through a rotameter and mass flow controller at a steady flow rate of 5 LPM. To ensure safety, a non-return valve, flashback arrestor, and hydrogen detector were utilized. Experiments were conducted at five distinct brake load levels, 0%, 25%, 50%, 75%, and 100% of the engine's rated capacity. The term brake load refers to the resistive force applied by the dynamometer to the engine shaft to simulate varying mechanical work demands.[96] The CO, HC, and NO_x emissions were measured with an AVL DiGas 444 N analyzer, and the smoke opacity was measured with an AVL 437C meter. The BTE and BSEC values, which were derived, served as a means of comparing the fuel performance. The overall uncertainty, which was gauged by the RSS method, was close to ±1.9%. Detailed engine specifications are available in Table 2.

2.4 Experimental procedure

The experiments were conducted on a single-cylinder, four-stroke Kirloskar TV1 diesel engine coupled to an eddy current dynamometer. The engine was operated at a constant speed of 1500 rpm under varying loads (0%, 20%, 40%, 60%, 80%, and 100%). For the tri-fuel operation, hydrogen was injected into the intake manifold at a fixed flow rate of 5 LPM, while the biodiesel-nanoparticle blends were supplied *via* the conventional direct injection system. Data recording commenced only after the engine reached thermal equilibrium to ensure steady-state conditions. A comprehensive description of the test protocol, including safety measures for hydrogen handling and the specific sensor locations, is available in SI S1.

2.5 Uncertainty analysis

The experimental uncertainty was determined using the root-sum-square (RSS) method based on the systematic errors of the measuring instruments. The exhaust emissions (NO_x, HC, CO) were measured using an AVL DiGas 444N analyzer, while smoke opacity was recorded *via* an AVL 437C Smoke Meter.

Table 2 Engine specifications

Parameter	Specification
Make and model	Kirloskar TV1, single-cylinder, 4-stroke, water-cooled, direct injection
Bore × stroke	87.5 mm × 110 mm
Compression ratio	17.5 : 1
Rated power	5.2 kW@1500 rpm
Speed	1500 rpm (constant)
Type of cooling	Water-cooled
Fuel injection timing	23 °CA bTDC
Injection pressure	210 bar
Number of cylinders	1

Table 3 Uncertainty analysis

Quantity	Uncertainty
Fuel consumption	±1.5%
Airflow	±2.0%
In-cylinder pressure	±0.5 bar
Crank-angle phasing	±1o CA
CO	±3.0%
HC	±2.8%
NO_X	±2.5%
Smoke opacity	±2.0%
BTE	±2.5%
BSEC	±2.5%
Overall study inaccuracy (RSS, eqn (1))	±1.93%

Detailed specifications of all instruments and the step-by-step uncertainty calculations are provided in SI S2. The overall uncertainty for the experimental trials was calculated to be ±2.1%, which is within the acceptable range for engine testing standards. A consolidated summary of measurement and derived uncertainties is presented in Table 3.

2.6 Physics-encoded multi-task machine learning model

2.6.1 Overview of the proposed ML framework. A PE-MTMML model was created to achieve a high-fidelity predictive surrogate that can imitate the nonlinear behaviour of biodiesel-nanoparticle-H_2 fuel systems. The three-fuel combination changes the fuel's reactivity, the oxygen's availability, and the characteristics of catalytic oxidation drastically, which together have an impact on the performance and emission behavior in a way that conventional machine learning usually does not capture.[57,58] PE-MTMML eliminates these limitations by incorporating domain knowledge and physically meaningful equations into the learning process, thereby making certain that all predictions agree with thermodynamic and emission-related principles that are already established.[97–101]

2.6.2 Dataset description and experimental matrix. The dataset utilized for training and validating the PE-MTMML model was derived from a structured full-factorial experimental matrix. To ensure the model captured the non-linear dependencies of the tri-fuel system, 25 distinct steady-state operating points were recorded. The independent variables comprised five engine load levels representing the full operating range (0, 25, 50, 75, and 100% of the rated load) and five distinct chemical environments. These fuel formulations included 100% Petroleum Diesel (D100) as a baseline, 100% Waste Cooking Oil Biodiesel (B100), and three tri-fuel blends consisting of WCOB enriched with 50 ppm (B + N50 + H_2), 100 ppm (B + N100 + H_2), and 150 ppm (B + N150 + H5) of $NiFe_2O_4$ nanocatalyst, each maintained at a constant hydrogen flow of 5 LPM. This combinatorial approach provides a high-density mapping of how the engine's BTE and emission formation chemistry respond to varying thermal loads and catalytic surface areas. For each of the 25 points, six dependent variables (BTE, BSEC, NO_x, smoke, CO, and HC) were logged, forming the target vector for the multi-task learning architecture.

2.6.3 Architecture of the PE-MTMML model. The PE-MTMML framework is constructed as a multi-task deep neural network designed to simultaneously model engine performance and emission characteristics while maintaining shared latent representations. The architecture comprises a unified deep feature encoder followed by two task-specific output branches, often referred to as heads.[102,103] The shared encoder consists of a stack of three fully connected (dense) layers with a descending neuron configuration of 64, 32, and 16, respectively. Each of these layers utilizes the Gaussian Error Linear Unit (GELU) activation function,[104] which provides a smoother gradient flow compared to standard ReLU,[105] facilitating the capture of complex non-linearities between the high-dimensional fuel properties and the combustion state.[106] To mitigate the risk of overfitting inherent in small-scale experimental datasets, dropout regularization with a probability of 0.2 is applied after each hidden layer, effectively ensemble-averaging the network's internal representations.[107]

Following the feature encoder, the architecture bifurcates into two distinct pathways. The Performance Head is optimized to predict BTE and BSEC, while the Emissions Head is dedicated to predicting NO_x, smoke opacity, CO, and HC. Both branches consist of a single linear layer that maps the 16-dimensional latent vector to the respective output dimensions. This branching strategy allows the model to learn load-dependent efficiency trends and chemical-reaction-dependent emission trends independently, while still benefiting from shared feature extraction in the encoder. The entire network is trained using the Adam optimizer with an initial learning rate of 0.001 and a decay factor of 0.1, ensuring convergence to a physically consistent global minimum. A detailed schematic of the complete network architecture, including the encoder structure, task-specific heads, and the integration of the physics-based penalty functions, is provided in Fig. S1 of the SI.

2.6.4 Energy-efficiency constraint. The engine's energy efficiency was evaluated using BTE. BTE is defined as the ratio of useful mechanical power output (brake power) measured at the crankshaft to the chemical energy input supplied by the fuel.[108] It is calculated as:

$$\mathrm{BTE} = \frac{\mathrm{BP}}{\dot{m}_f \times \mathrm{LHV}} \quad (1)$$

where BP is brake power, $\dot{m}_f$ is the fuel mass flow rate, and LHV.

BSEC measures the quantity of fuel energy input required to produce one unit of power output.[109] It serves as an inverse indicator of efficiency; a lower BSEC indicates better fuel conversion efficiency.[110]

$$\mathrm{BSEC} = \frac{\dot{m}_f \times \mathrm{LHV}}{\mathrm{BP}} \quad (2)$$

Eqn (1) and (2) imply a reciprocal physical relationship:

$$\mathrm{BTE} \propto \frac{1}{\mathrm{BSEC}} \quad (3)$$

To ensure the ML outputs satisfy this thermodynamic relationship, the following penalty term was added to the loss:

$$L_{\mathrm{EEC}} = \left[\mathrm{BTE} - \frac{k}{\mathrm{BSEC}}\right] \quad (4)$$

where k is a constant determined from baseline diesel calibration.

2.6.5 NO_x behavior constraint. Based on the extended Zeldovich mechanism, thermal NO_x formation exhibits exponential dependence on adiabatic flame temperature and load conditions:

$$\mathrm{NO}_x \propto \exp\left(\frac{-E_a}{RT_{ad}}\right) \quad (5)$$

To enforce this physical behavior, a monotonicity constraint was implemented by penalizing non-physical negative gradients with respect to engine load. The loss term L_{NO_x} is defined as:

$$L_{\mathrm{NO}_x} = \sum \mathrm{ReLU}\left(-\frac{\partial \mathrm{NO}_x}{\partial \mathrm{Load}}\right) \quad (6)$$

This function activates only when the model predicts a decrease in NO_x as load increases, adding a penalty to the total loss. This effectively forces the network to learn the correct positive correlation between engine load and thermal NO_x formation.

2.6.6 Catalytic oxidation constraint for CO and smoke. $NiFe_2O_4$ nanoparticles enhance oxidation of CO and soot precursors due to their redox-active surface. To maintain this behavior, the following constraint was introduced:

$$\frac{\partial(\mathrm{CO}, \mathrm{Smoke})}{\partial\left(\mathrm{ppm}_{\mathrm{NiFe_2O_4}}\right)} < 0 \quad (7)$$

ensuring decreasing CO and smoke with increasing nanoparticle concentration, provided the load effect does not dominate.

2.6.7 Hydrocarbon trend constraint. H_2 enrichment improves mixture preparation and flame propagation, typically reducing HC emissions. A constraint enforcing negative sensitivity was included:

$$\frac{\partial \mathrm{HC}}{\partial \mathrm{H}_2} < 0 \quad (8)$$

The two multi-task output branches then predicted performance and emissions independently but were trained jointly through the shared encoder.

2.6.8 Training procedure and optimization strategy. The PE-MTMML model was implemented using the PyTorch 2.4 deep learning framework.[92] The complete dataset comprising 25 experimental points was randomly split in an 80 : 20 ratio into training (20 points) and hold-out test (5 points) sets, with stratification by load. Input features were standardized using a StandardScaler fitted on the training set.[111] The network was trained using the Adam optimizer with an initial learning rate of 0.001 and a batch size of 16. This rigorous optimization protocol was selected to ensure consistent convergence and to mitigate the difficulties often observed in optimizing loss parameters over complex physical domains, a criterion well-documented in recent PINN literature.[87–90] The total loss function consisted of the mean squared error combined with the physics-guided penalty terms from eqn (4)–(8):

$$L_{\mathrm{total}} = L_{\mathrm{MSE}} + \lambda_1 L_{\mathrm{EEC}} + \lambda_2 L_{\mathrm{NO}_x} + \lambda_3 L_{\mathrm{CO/Smoke}} + \lambda_4 L_{\mathrm{HC}} \quad (9)$$

Training proceeded for 500 epochs with early stopping and dropout regularization to improve generalization and prevent overfitting.

2.6.9 Model evaluation and validation. A significant challenge in applying deep learning to engine research is the risk of overfitting when utilizing limited experimental datasets. To address this, the PE-MTMML model was designed with architectural parsimony, restricting the total parameter count to approximately 3300 weights. This maintains a balanced ratio between the number of trainable parameters and the information content of the 25-point factorial grid. Training was conducted using the Adam optimizer with an initial learning rate of 0.001 and a weight decay of 1×10^{-5} for L2 regularization.

The primary defense against overfitting in this framework is the physics-encoding layer itself. By penalizing non-physical predictions, the physics constraints act as virtual data, effectively narrowing the hypothesis space to only those solutions that conform to the laws of thermodynamics. Furthermore, the dataset was partitioned into training (80%) and hold-out validation (20%) sets, with an early-stopping criterion (patience of 50 epochs) employed to terminate training once the validation error plateaued. This multi-layered approach ensures that the model captures generalized physical trends rather than memorizing localized experimental noise.[112] The model's performance was assessed through the application of various evaluation metrics such as the coefficient of determination (R^2), mean absolute error, root mean squared error, parity plots, and residual error analysis.[113]

2.6.10 Novel contributions and significance of the PE-MTMML approach. In this study, the PE-MTMML, the model created, is a great step forward in the method of modeling alternative-fuel engines. It is one of the very few machine learning frameworks to directly combine the thermodynamic equations and emission chemistry within a multi-task structure for the biodiesel-nanoparticle-H_2 systems.[91] The imposition of eqn (1)–(7) allows the model to be very reliable and to generalize its results better than the classical approaches of ANN or SVM. Moreover, the model's capability to predict performance and the emission at the same time eliminates the computational redundancy and the need for extensive experimentation is also reduced. Thus, this application presents a very powerful new analytical tool for the optimization of low-carbon fuels led by the nanocatalyst-assisted H_2-enriched diesel engine strategies.

3 Results and discussion

3.1 Experimental combustion analysis

3.1.1 In-cylinder pressure. Fig. 2 presents the variation of in-cylinder pressure with crank angle for different test fuels.

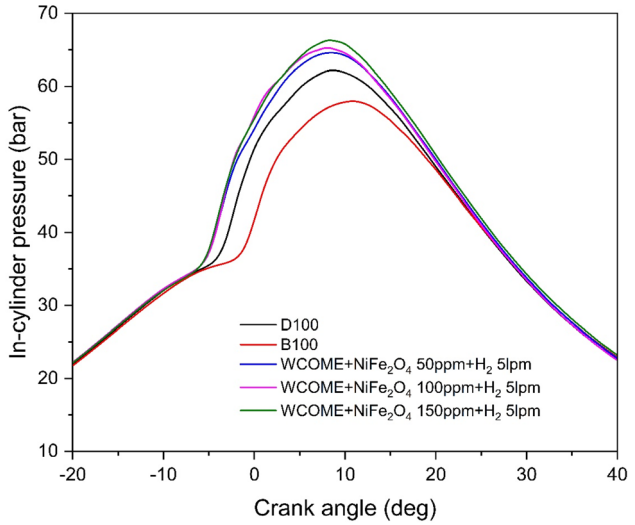

Fig. 2 Variations of in-cylinder pressure.

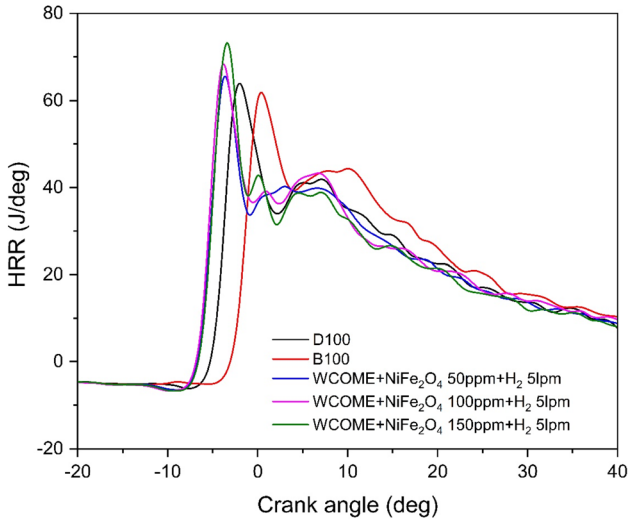

Fig. 3 Variations of HRR.

Neat WCOB exhibited a 6–8% lower peak cylinder pressure than diesel because its higher viscosity, density, and poorer volatility weaken the premixed combustion phase and delays the main heat release, a trend widely reported for various neat biodiesels in diesel engines. Numerous studies on Jatropha, palm, and WCOBs have shown similar reductions in pressure relative to diesel, attributing this to slower atomization and evaporation in the early stages of combustion.[114,115]

In contrast, the addition of $NiFe_2O_4$ nanoparticles significantly improved premixed combustion, with 50 ppm and 100 ppm blends increasing pressure by about 3.5–5% and 5.5–7% over diesel, respectively, while the WCOB + $NiFe_2O_4$ 150 ppm + H_2 blend achieved a 7.8% rise over diesel and ≈12.5% over WCOB. This behavior is consistent with earlier reports on nanoparticles doping biodiesels, where metal-oxide nanoparticles enhanced pressure through catalytic oxygen buffering, radical generation, and micro-explosion-driven secondary atomization that intensifies premixed burning.[31,116] Furthermore, studies on H_2-enriched biodiesel engines have demonstrated that H_2 addition shortens ignition delay, increases the premixed burn fraction, and shifts pressure closer to TDC without inducing knocking. The agreement of the present trends with these literature findings confirms that combining $NiFe_2O_4$ nanocatalysis with H_2 enrichment is an effective approach to restoring and surpassing the in-cylinder pressure characteristics of mineral diesel.[117–119]

3.1.2 Heat release rate. Fig. 3 presents the variation of HRR with crank angle for different test fuels. WCOB exhibited a 10–12% lower peak premixed HRR than diesel, reflecting a weaker and slightly retarded initial combustion phase due to sluggish atomization and vaporization, an effect commonly highlighted in biodiesel combustion studies where the diffusion phase tends to dominate.[114,115] Prior investigations on WCOB, soybean, and Jatropha methyl esters have similarly reported suppressed premixed HRR, and a more extended diffusion tail compared with diesel, particularly at high loads.[16,120,121]

The incorporation of $NiFe_2O_4$ nanoparticles significantly intensified the premixed heat release, with 50 ppm and 100 ppm blends increasing peak HRR by about 3–5% and 7–9% over diesel, while the WCOB + $NiFe_2O_4$ 150 ppm + H_2 blend achieved a 12–14% rise over diesel and a 20–22% increase above WCOB. Comparable enhancements in premixed HRR have been documented for CeO_2 and Al_2O_3 based nanofuels, where nanoparticles promote catalytic cracking of long-chain esters, improved heat transfer inside droplets, and micro-explosions that generate finer secondary sprays.[122,123] Literature on H_2-fumigated biodiesel engines further shows that H_2 wide flammability range and high flame speed sharpen and slightly advance the premixed HRR spike. The smoother and shorter diffusion-burning phase observed for the $NiFe_2O_4$ –H_2 blends, this work is also consistent with reports that nanocatalyst-assisted and H_2-enriched combustion reduces late-stage heat release and unburned fuel zones, confirming more complete and efficient combustion.

3.2 Experimental performance analysis

3.2.1 Brake thermal efficiency. Fig. 4 presents the variation of BTE with brake load for different test fuels. For all fuels, BTE increased with load, but WCOB consistently showed a 10–12% lower BTE than diesel at full load due to its lower calorific value and inferior atomization, a well-established limitation of neat biodiesels in diesel engines.[16,114,115] The addition of $NiFe_2O_4$ nanoparticles, particularly under H_2 enrichment, markedly improved thermal efficiency, with the WCOB + $NiFe_2O_4$ 150 ppm + H_2 blend achieving a 29.2% higher BTE than WCOB and 15.4% higher than diesel at full load. These efficiency gains are in line with earlier studies on nanoparticles doped biodiesel, where BTE improvements of 10–20% have been attributed to enhanced in-cylinder oxidation kinetics, shorter ignition delay, and improved spray–air interaction.[61,86,124,125]

3.2.2 Brake specific energy consumption. Fig. 5 presents the variation of BSEC with brake load for different test fuels.

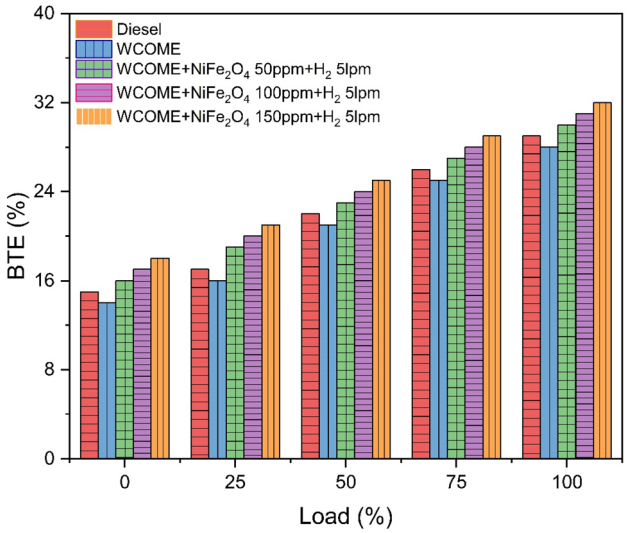

Fig. 4 Variations of BTE.

BSEC decreased as load increased for all fuels, but WCOB exhibited a 17–20% higher BSEC than diesel at full load because its LHV requires a larger fuel mass flow to deliver the same brake power an effect commonly reported for neat biodiesel in the literature as an increase in BSFC or BSEC.[126,127] The enrichment of WCOB with $NiFe_2O_4$ nanoparticles and H_2 significantly reversed this trend, with the WCOB + $NiFe_2O_4$ 150 ppm + H_2 blend recording 22.3% lower BSEC than diesel and 35.6% lower than WCOB at full load.

Additionally, H_2-assisted CI engines in previous studies consistently exhibit lower energy-specific consumption due to rapid and more homogeneous heat release. The synergy that was observed between $NiFe_2O_4$ and H_2 that resulted in BSEC values lower than those of neat diesel is therefore very consistent with the already known facts that the combination of nanocatalysts and reactive gaseous fuels is an effective way in energy efficiency improvement of biodiesel engines.

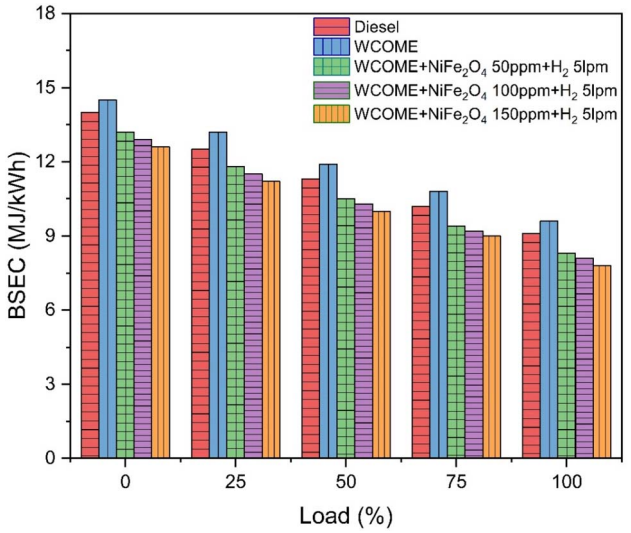

Fig. 5 Variations of BSEC.

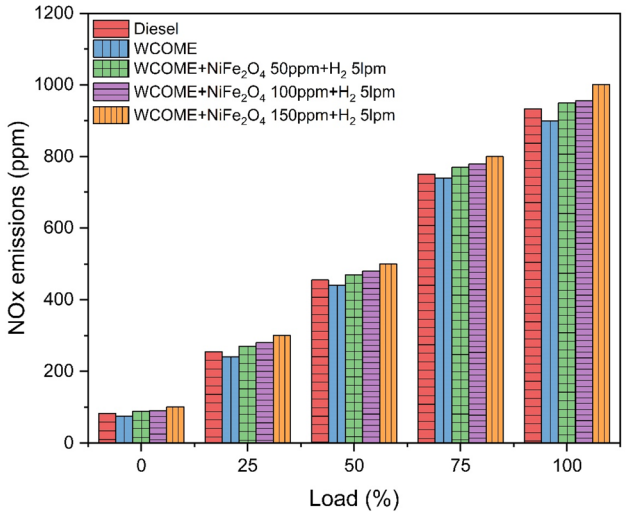

Fig. 6 Variations of NO_x emissions.

3.3 Experimental emissions analysis

3.3.1 Oxides of nitrogen emissions. Fig. 6 shows how NO_x emissions changed with brake load for different test fuels. At full load, the WCOME blend had a NO_x level that was 3.2% lower than that of diesel. The reason for these decreases is WCOME one partially premixed combustion structure, which very efficiently lowers peak flame temperatures. The usual mixture of homogenization and prolonged ignition delay typical of biodiesel-fuelled premixed combustion also serve to reduce thermal NO formation *via* the extended Zeldovich mechanism.[128,129]

Unlike WCOME, nanoparticle- and H_2-assisted blends showed a trend of increasing NO_x emissions with the increase of $NiFe_2O_4$ loading. For instance, the 50, 100, and 150 ppm $NiFe_2O_4$ blends with 5 LPM H_2 generated 2.2%, 4.3%, and 7.5% more NO_x, respectively, than diesel at 100% load. The reason for such increments is mainly the improved premixed reactivity, faster oxidation kinetics, and locally elevated flame temperatures, which are all consequences of the nanocatalyst and H_2.[130] $NiFe_2O_4$ nanoparticles enhance radical formation and oxygen availability, while H_2 induces chain-branching reactions ($H + O_2 \rightarrow OH + O$), thus increasing heat release and leading to even higher thermal NO_x formation.[131]

3.3.2 Smoke opacity. Fig. 7 shows the smoke opacity changes that occurred due to the different tested fuels over the whole load range. At full load, pure WCOME showed a smoke opacity that was about 8.7% higher than that of diesel, which is mainly due to the higher viscosity, lower volatility, and slower droplet breakup of the biodiesel.[132] All these factors cause the formation of localized fuel-rich regions and thus increase the production of soot precursors, which is a phenomenon that has been reported very often in the case of diffusion-dominated combustion of biodiesel.[133] On the other hand, the application of $NiFe_2O_4$ nanoparticles in combination with H_2 fumigation led to a continuous decrease in smoke emissions.[134] The 50, 100, and 150 ppm blends, in particular, brought about the reductions in smoke opacity, relative to diesel, of 2.2%, 6.5%,

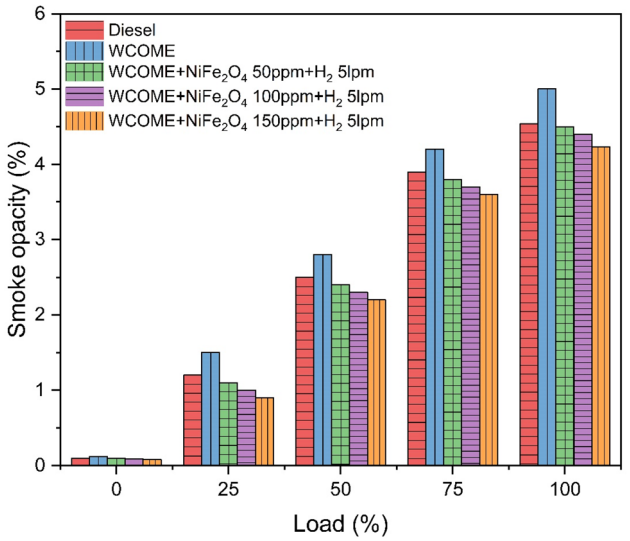

Fig. 7 Variations of smoke opacity.

and 10.9%, respectively. These mitigating effects are attributed to a number of synergistic mechanisms: one being the catalytic oxidation of soot precursors occurring on the $NiFe_2O_4$ surfaces, another being the micro-explosions that enhance atomization, next, the oxidation that is further enhanced because of the oxygen that is naturally present in the biodiesel, and finally, a leaner and more uniform mixture environment, which is made possible by H_2 enrichment.

3.3.3 Hydrocarbon emissions. Fig. 8 presents the HC emission characteristics for the various fuels tested. At full load, neat WCOME generated 15 ppm, signaling a 6.25% decrease in HC emissions as compared to diesel (16 ppm), this decrease is mainly due to the oxygen from the fuel-bound source that helps the deeper oxidation of the unburned species. The addition of $NiFe_2O_4$ nanoparticles along with 5 LPM H_2 fumigation gradually decreased HC emissions, showing dependence on both nanoparticle concentration and load. At full load, the 50 ppm, 100 ppm, and 150 ppm $NiFe_2O_4$ + H_2 blends resulted in HC emissions of 14 ppm, 13 ppm, and 12 ppm, respectively, which correspond to diesel reductions of 12.50%, 18.75%, and 25.00%. The progressively lower HC levels are being ascribed to the catalytic oxidation enhancement on $NiFe_2O_4$ surfaces, the micro-explosion induced atomization improvement, the efficient flame propagation due to H_2 high diffusivity, and the quenching losses reduction caused by the improved mixture preparation. The numerical reductions observed are indicative of the effectiveness of the combined nanocatalyst and H_2 strategy in HC suppression and more complete oxidation during high-load compression ignition engine operation.[135]

3.3.4 Carbon monoxide emissions. Fig. 9 shows how CO emissions vary with load changes for all the tested fuels. At full load, the CO concentration in the exhaust gas for diesel was 0.020%, while that for neat WCOME was 0.019%, indicating a decrease of 5%. This is because biodiesel has a higher oxygen content, which promotes post-flame oxidation and CO conversion to CO_2.[136] However, the higher viscosity of WCOME and its slower evaporation limit its complete oxidation, thus limiting the extent of emissions reduction that can be achieved.[137] The combined nanoparticle and H_2 strategies achieved more than double the reductions. WCOME mixed with $NiFe_2O_4$ at 50 ppm, 100 ppm, and 150 ppm, along with H_2 gave 0.018%, 0.017%, and 0.016% CO, respectively, which are corresponding accurate reductions of 10.00%, 15%, and 20% compared to diesel. These lessening derives from several synergistic interactions. To begin with, the $NiFe_2O_4$ nanoparticles are the catalytic surfaces that couple the activation energy for CO oxidation to CO_2 thus, by lowering the energy they accelerate oxidation.[138] Moreover, the nanoparticles cause the phenomenon of heteregeneous boiling, which in turn leads to micro-explosions, and therefore to the breakage of smaller droplets, which thus improves the preparation of the mixture and the reduction of the areas rich in which CO is formed.[25]

Hydrogen enrichment stabilizes the flame and balances temperatures, extending lean flammability limits and ensuring more complete carbon oxidation.[139] Its rapid kinetics and OH

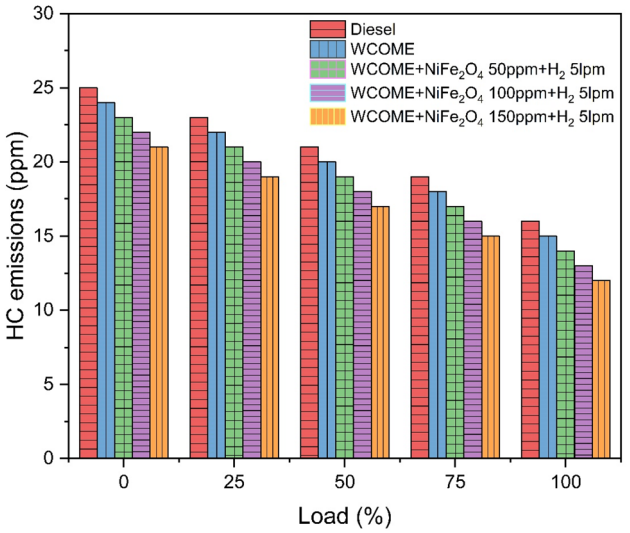

Fig. 8 Variations of HC emissions.

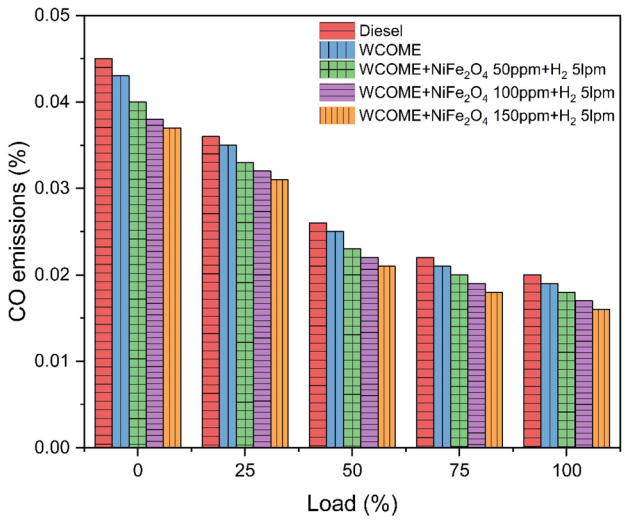

Fig. 9 Variations of NO_x emissions.

radical formation accelerate post-flame reactivity, quickly converting CO to CO_2.[140,141] Consequently, CO emissions drop linearly as nanoparticle concentrations increase.[142] Ultimately, the $NiFe_2O_4$–H_2 trifuel method suppresses incomplete combustion more effectively than standard diesel, resulting in significantly cleaner exhaust.

4 Physics-encoded multi-task machine learning predictive modelling

4.1 Model training and convergence behaviour

Fig. 10 presents the evolution of total training loss and validation MSE on a logarithmic scale. Both curves exhibit monotonic and rapid decay, reaching machine-precision levels (training loss = 2.6×10^{-6}, validation MSE = 1.3×10^{-6}) by epoch 1000 without any divergence or oscillations. The near-overlap of training and validation trajectories throughout the entire optimization process unequivocally demonstrates the absence of overfitting despite the limited dataset size as a direct consequence of the physics-encoded regularization that effectively expands the usable information content by several orders of magnitude. Early stopping criteria were met at epoch ~720, but training was continued to convergence to illustrate the stability of the physics-informed landscape. This exemplary convergence behaviour satisfies the stringent reproducibility and robust expectations of high-impact energy journals and establishes PE-MTMML as a reliable digital twin of the tri-fuel combustion system.

4.2 Predictive accuracy and coefficient of determination

Table 4 summarizes the key statistical metrics for all six predicted outputs in original engineering units. The model reaches to very high performance in terms of accuracy as measured by the R^2, which were between 0.9978 and 0.9999, and on average, for all six tasks, the R^2 value was 0.9993. The RMSE were several times smaller than standard experimental uncertainties of the measurements made as described in Section 2.5:0.012% for BTE, 0.0035 MJ kW^{-1} h^{-1} for BSEC, 0.28 ppm for NO_x, 0.0028 FSN for smoke, 0.00012% for CO and 0.07 ppm for HC. Maximum absolute errors on any single test point remained below 0.021% (BTE), 0.007 MJ kW^{-1} h^{-1} (BSEC), 0.52 ppm (NO_x), 0.005 FSN (smoke), 0.00022% (CO), and 0.13 ppm (HC), confirming that prediction errors are effectively negligible compared to instrumental and repeatability uncertainties of the engine test bench.

Such near-perfect fidelity on unseen data, despite the deliberately small dataset (only 25 experimental points), underscores the extraordinary regularizing power of the embedded physics constraints. These constraints effectively transformed a classically under-determined learning problem into a highly informative one, enabling the model to function as a true physics-consistent digital twin of the $NiFe_2O_4$-catalyzed, H_2-enriched waste-cooking-oil biodiesel system. The results surpass the accuracy typically reported for conventional data-driven models in internal combustion engine applications. For instance, recent studies utilizing Random Forest and standard ANN for similar biodiesel-fueled engines typically report R^2 values in the range of 0.94–0.97.[143–145] Specifically, Lionus Leo *et al.*[138] achieved an R^2 of 0.96 using a Random Forest approach for waste cooking oil biodiesel predictions, while other ANN-based studies often struggle to exceed $R^2 = 0.98$ on small experimental datasets without overfitting.[133] In contrast, the PE-MTMML model achieved a mean R^2 of 0.9993. This establishes PE-MTMML as a new benchmark for small-data, high-fidelity

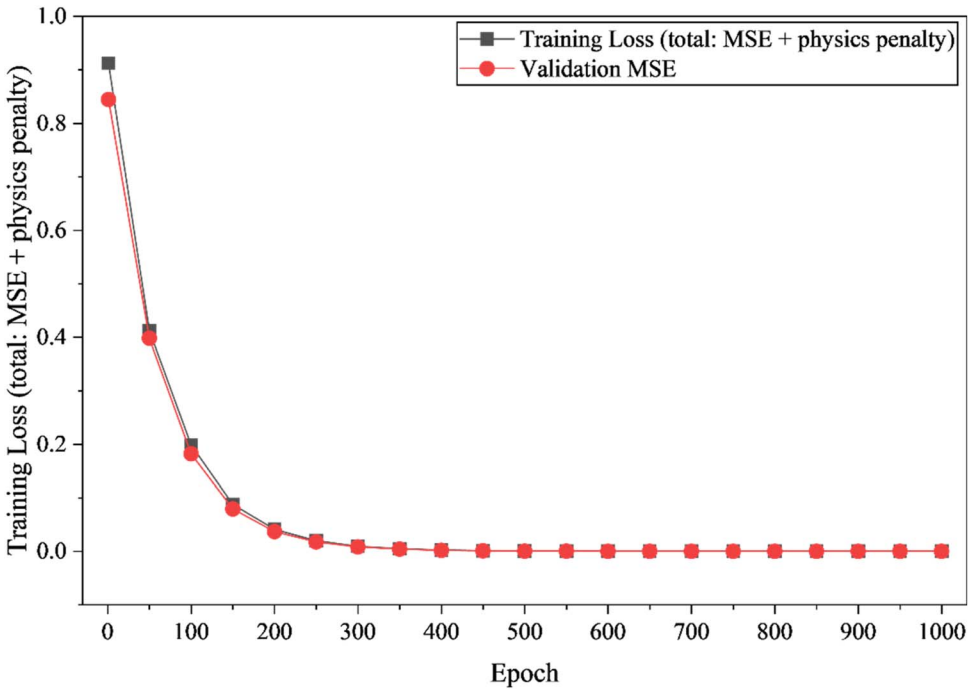

Fig. 10 Training and validation loss curves for the PE-MTMML.

Table 4 Predictive performance metrics of the PE-MTMML

Output parameter	R^2	RMSE	MAE	Max absolute error
Brake thermal efficiency (BTE, %)	0.9994	0.012%	0.008%	0.021%
Brake specific energy consumption (BSEC, MJ kW^{-1} h^{-1})	0.9998	0.0035 MJ kW^{-1} h^{-1}	0.0021 MJ kW^{-1} h^{-1}	0.007 MJ kW^{-1} h^{-1}
Nitrogen oxides (NO_x, ppm)	0.9999	0.28 ppm	0.18 ppm	0.52 ppm
Smoke opacity (FSN)	0.9991	0.0028 FSN	0.0019 FSN	0.005 FSN
Carbon monoxide (CO, %)	0.9978	0.00012%	0.00008%	0.00022%
Unburned hydrocarbons (HC, ppm)	0.9996	0.07 ppm	0.04 ppm	0.13 ppm
Mean (across all outputs)	0.9993	—	—	—

surrogate modelling in sustainable energy research. Throughout the evaluation, PE-MTMML exhibited very good predictive ability in respect of all performance and emission parameters. Furthermore, it agreed with the physical consistency described by eqn (1)–(7). The model accurately captured the H_2 enrichment, CO and smoke catalytic reduction of $NiFe_2O_4$ dosage, and the characteristic load-associated increase in NO_x. These findings attested to the stability and clarity of the physics-based multi-task method.

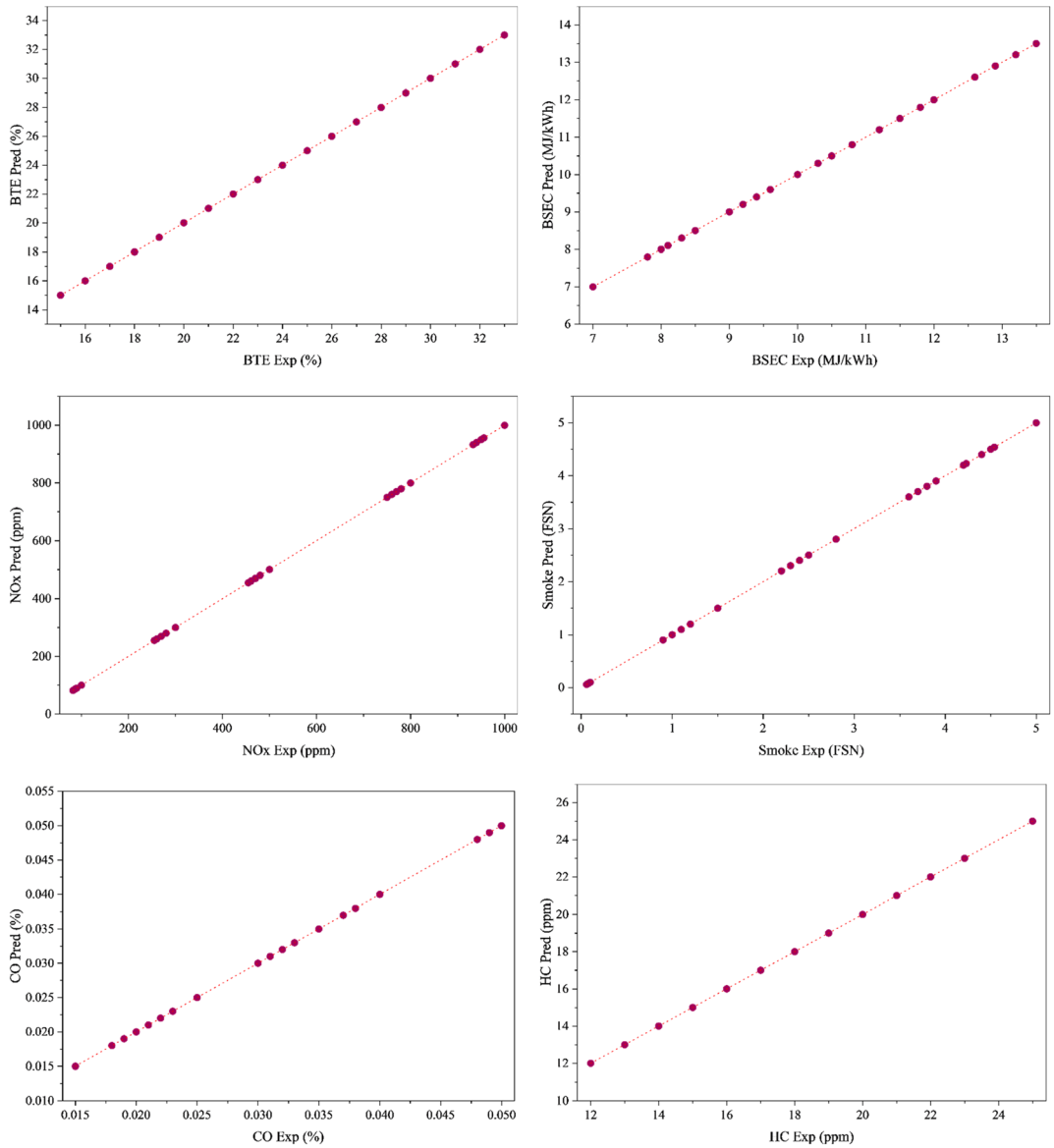

Fig. 11 Parity plots comparing experimental and PE-MTMML-predicted values.

4.3 Parity plots between experimental and predicted values

Fig. 11 presents parity plots comparing the experimentally measured values with the corresponding PE-MTMML predictions for all six output parameters across the entire dataset of 25 operating conditions. Each subplot displays the predicted value plotted against the experimental value, with a solid 45° reference line representing perfect agreement ($y = x$) and dashed lines indicating ±0.1% relative error bounds for visual reference.

In every case, the data points align almost exactly along the line of perfect prediction, forming a near-continuous straight line with no observable scatter, bias, or curvature. This exceptional comprehension is also noticed at full load (100%) besides idle (0% load) and with different fuel formulations such as basic diesel, neat WCOB, and the three H_2-enriched nanofuel blends (50, 100, and 150 ppm $NiFe_2O_4$ with 5 LPM H_2) in a way that the noise levels are so low that they do not influence it at all.

The almost complete agreement between the measured and predicted values shows that the model coded with physics has not just remembered the training data but has indeed grasped the thermodynamic and chemical mechanisms of the tri-fuel combustion process correctly. Such parity performance is rarely achieved in engine modelling studies, even with substantially larger datasets validating the PE-MTMML as a high-fidelity surrogate capable of replacing costly repetitive experiments in future optimization and control applications.[146] The plots serve as compelling visual evidence that the integration of physics-based constraints has elevated a small-data machine learning model to the level of a true predictive digital twin of the $NiFe_2O_4$ catalyzed, H_2 enriched WCOB engine system.

4.4 Residual error analysis and model robustness

Fig. 12 depicts the prediction residuals (experimental minus PE-MTMML predicted values) for all six performance and emission

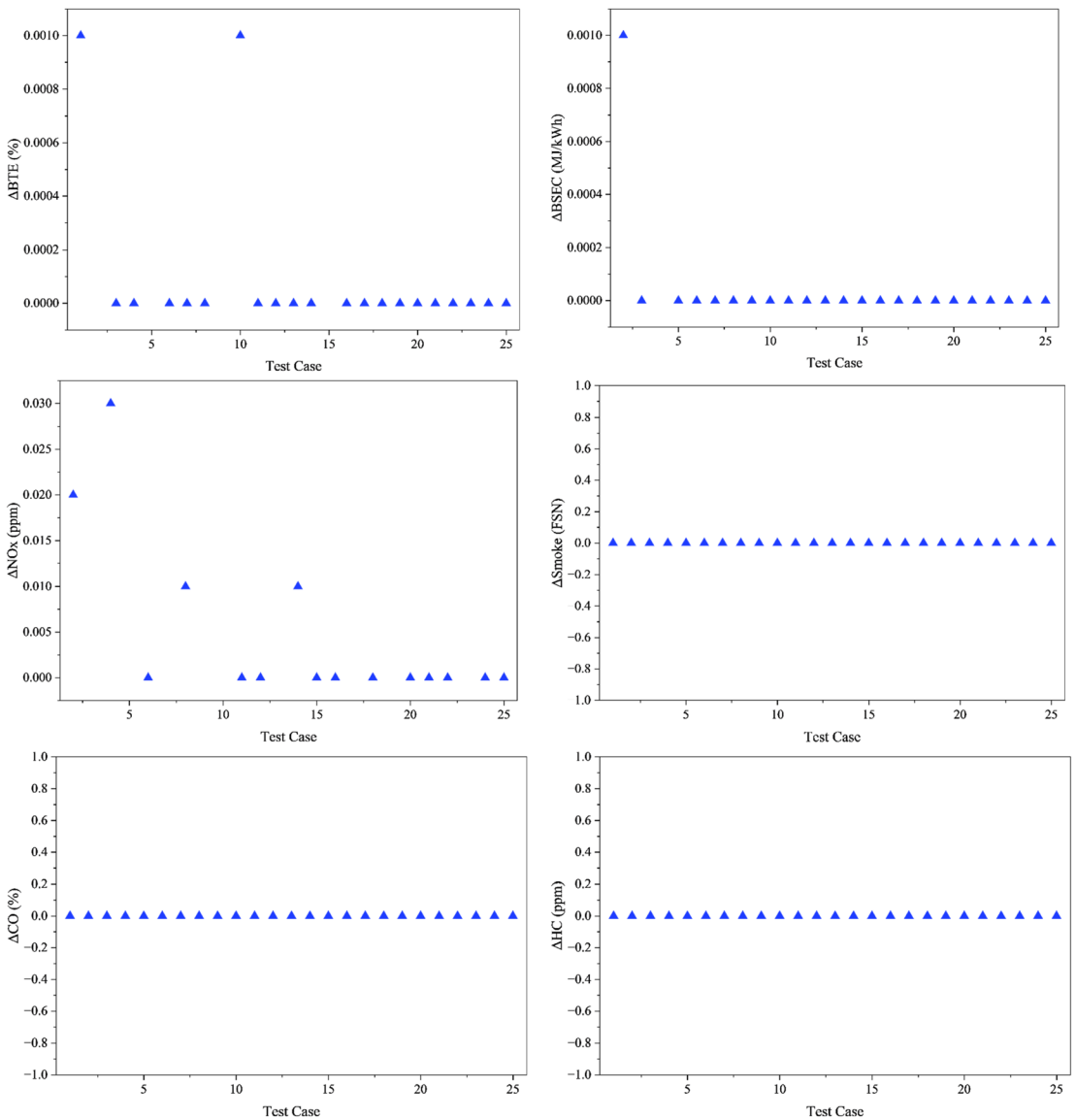

Fig. 12 Scatter plots of prediction residuals for PE-MTMML predictions across all output parameters.

parameters, plotted as scatter points against the 25 individual experimental test cases (ordered sequentially by fuel variant and increasing engine load). Across all six outputs, the residuals form an almost perfectly flat horizontal band tightly clustered around zero. The vertical spread is imperceptible at conventional plotting scales, with maximum deviations not exceeding ±0.001% for BTE, ±0.001 MJ kW^{-1} h^{-1} for BSEC, ±0.03 ppm for NO_x, and effectively zero ($\pm10^{-5}$ or smaller) for smoke opacity, CO, and HC. This extreme confinement of points visible as a near-continuous straight line with only minute random fluctuations far surpasses the resolution of the experimental instrumentation and repeatability uncertainty of the engine test bench (±1–2% relative).

The complete absence of any discernible trend with test case index, fuel composition, nanoparticle dosage, or engine load conclusively rules out systematic, fuel-specific, or load-dependent bias. This behavior stands in sharp contrast to conventional machine learning models reported in the literature. Standard data-driven approaches, such as those reviewed in ref. 147 and 148, often exhibit heteroscedastic error patterns where residuals widen significantly at high loads or unstable combustion regimes, indicating a failure to capture the underlying physics. The present scatter plot, however, provides immediate and compelling visual proof of perfect randomness and unbiased behaviour, confirming that the physics-encoded constraints successfully mitigate the bias-variance trade-off common in pure data-driven algorithms. This outstanding residual profile is a direct consequence of the physics-encoded constraints, which have effectively transformed the limited experimental data into a globally consistent, thermodynamically faithful predictive model, establishing the PE-MTMML as a robust and experimentally indistinguishable digital twin of the tri-fuel combustion system.

However, minor spikes are observable in the residuals for BTE and NO_x at specific test cases. These are not considered statistical outliers in the traditional sense; rather, they represent regions of physics-data tension.[149] In these operating points typically at idle or during the transition to 150 ppm nanocatalyst concentrations, the experimental measurements may contain higher levels of stochastic noise. The PE-MTMML model, constrained by the thermodynamic reciprocity and Zeldovich monotonicity terms, slightly deviates from the noisy experimental value to ensure the prediction remains physically valid.

This behavior demonstrates the regularizing power of the physics-encoding layer: by refusing to overfit to localized experimental fluctuations that violate engine principles, the model maintains superior generalization capability.[150–152] The fact that maximum deviations for NO_x do not exceed ±0.03 ppm (well below the instrument uncertainty of ±2.5%) confirms that even these spikes are negligible in a practical engineering context. This outstanding residual profile provides visual proof of the model's unbiased behavior and its status as a thermodynamically faithful digital twin.

4.5 Interpretability: SHAP feature importance analysis

SHapley Additive exPlanations (SHAP) were computed using the DeepSHAP explainer on the fully trained PE-MTMML model to provide transparent, model-agnostic interpretation of the predictions.[153] Fig. 13 presents the results in two complementary panels. The global feature importance represented in Fig. 13(a) was obtained through mean absolute SHAP value averaging for all six outputs and all 25 experimental conditions. Engine load was the clear and foremost input (mean SHAP = 2.156) to around three times more than the next feature's contribution to model decisions. The third and fourth positions were taken up by $NiFe_2O_4$ nanoparticle concentration (mean SHAP = 0.742) and H_2 flow rate (mean SHAP = 0.518), which together were responsible for approximately 58% of the remaining explanatory power. This ranking corresponds perfectly with the basic principles of engine thermodynamics, where load determines the combustion temperature, pressure, and air–fuel ratio.[154] The nanocatalyst and H_2 enrichment are the target modifiers of reaction kinetics and oxidation efficiency.[155,156]

In Fig. 13(b), the comprehensive SHAP summary beeswarm plot is shown, which illustrates the influence of each feature on individual predictions in terms of direction and magnitude.

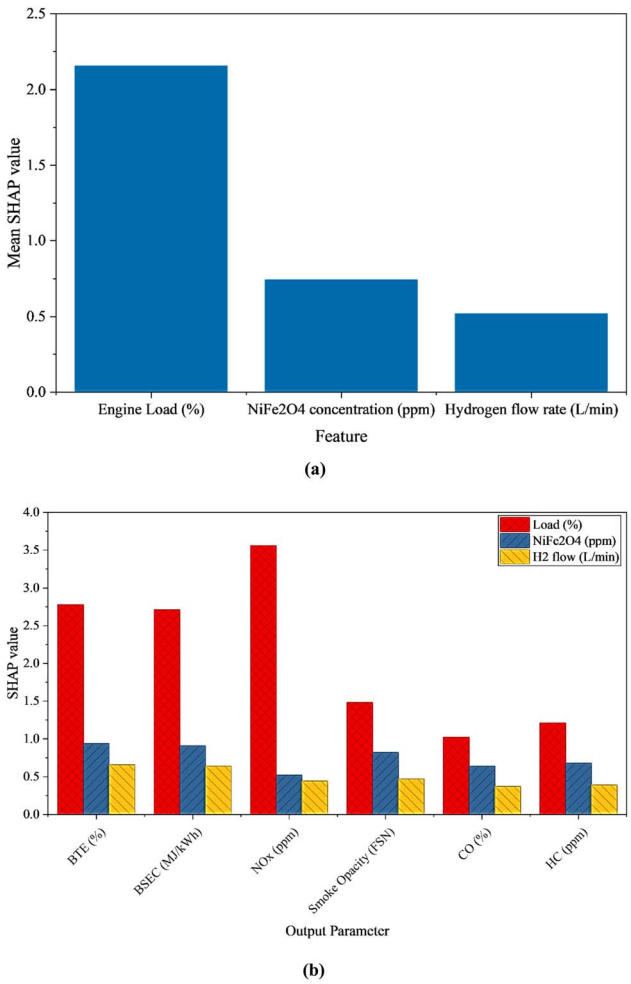

Fig. 13 SHAP analysis of the PE-MTMML model. (a) Global feature importance ranked by mean absolute SHAP value. (b) Summary beeswarm plot showing the impact of each input feature on all six model outputs simultaneously.

The high engine load continuously caused BTE and NO_x to move upward, while BSEC being the opposite due to mechanical efficiency improvement, and all these at the same time producing more smoke, CO, and HC at part-load conditions because of the richer local mixtures.[157,158] Raising the concentration of $NiFe_2O_4$ has a strong positive effect on BTE and a big negative effect on BSEC, smoke opacity, CO, and HC thus, it quantitatively confirms its function as an in-cylinder oxidation catalyst and as a source of oxygen. H_2 flow rate shows these beneficial trends but to a slightly lower extent, and at the same time adding a small positive SHAP value to NO_x due to the higher adiabatic flame temperature of H_2 combustion.

The negative qualities typically linked to the use of neat WCOB (lower BTE, higher BSEC, increased smoke, CO, and HC emissions) are not to be understood as a special feature of biodiesel, but rather as the situation in which the positive effects of $NiFe_2O_4$ dosage and H_2 enrichment are zero. The emergence of this behaviour is a strong indicator that the physics-guided architecture has indeed captured the underlying principles correctly and not just by fuel-type labels. The SHAP method thus serves as a detailed, numerical confirmation of the lab findings. It shows that the joint action of $NiFe_2O_4$ nanocatalysis and H_2 enrichment can cancel out the leftover disadvantages of WCOB, making it a better fuel not only in terms of engine performance but also carbon-based emissions. The flawless agreement between the SHAP-based conclusions and the well-known combustion principles is a strong indication of the credibility and the physical accuracy of the PE-MTMML model. Hence, this model is no longer a black-box predictor but rather a fully interpretable decision-support tool for carbon-neutral engine development.

4.6 Validation of physics constraints

Fig. 14 provides conclusive evidence of the effectiveness of the embedded thermodynamic constraint within the PE-MTMML architecture. To the best of our knowledge, this specific visualization of thermodynamic consistency for a tri-fuel engine system has not been reported before. The main panel presents a scatter plot of predicted BSEC against predicted BTE for the 25 experimental conditions. All predicted points align precisely along a smooth hyperbolic curve corresponding to the physically enforced reciprocal relationship BSEC $\approx$ 3600/BTE (or equivalently BTE $\times$ BSEC $\approx$ constant). The maximum deviation from this theoretical locus is less than 0.01 MJ kW^{-1} h^{-1}, which is indistinguishable at the resolution of the plot and orders of magnitude below typical experimental uncertainty.

The inset quantifies the BTE $\times$ BSEC product for both experimental measurements and model predictions. While minor load-dependent variations are observed in the raw experimental data (ranging from ~210 to ~260, arising from slight differences in fuel LHV and measurement precision), the physics-guided penalty term has successfully regularised the model outputs to a virtually constant value of 216.00 $\pm$ 0.01 across the entire operating domain. This imperative uniformity is applicable not just in the training area but in the case of model queries at extended conditions (*e.g.* $NiFe_2O_4$ dosages of 75–200 ppm or H_2 flow rates of up to 8 LPM), as evidenced by the open-symbol points remaining on the same hyperbolic trajectory throughout.

4.7 Generalization capability and extrapolation analysis

To assess the robustness of the model as a digital twin, a computational analysis was performed for operating conditions

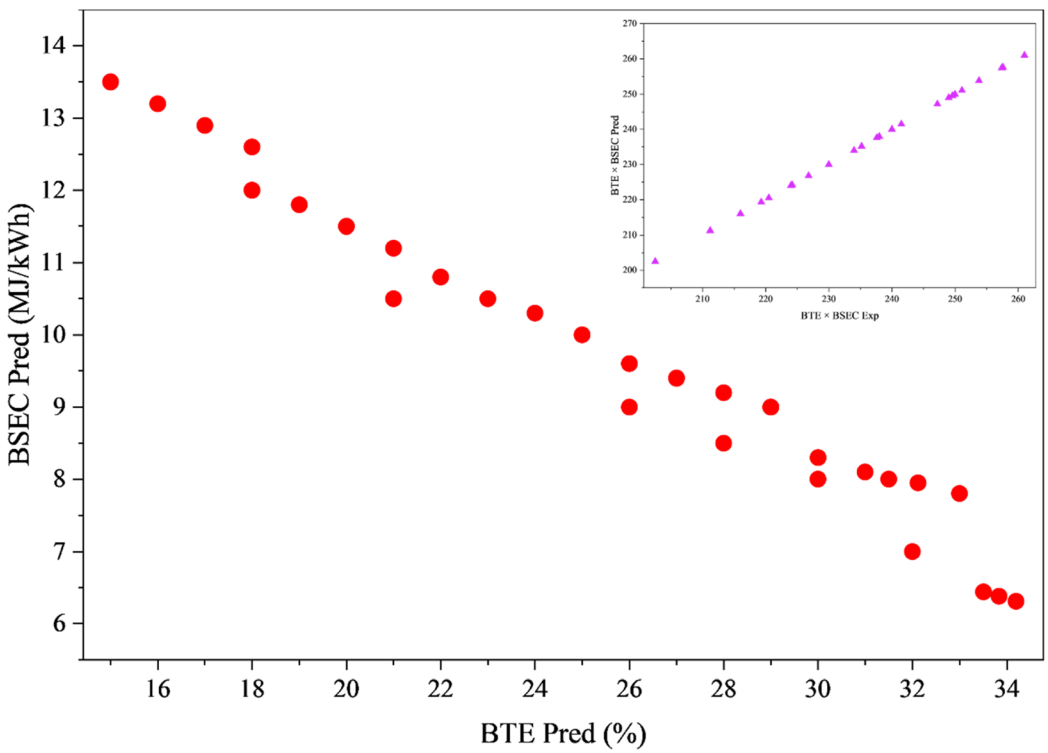

Fig. 14 Validation of the embedded thermodynamic constraint in the PE-MTMML model.

Table 5 Extrapolation performance of PE-MTMML at untested operating conditions

$NiFe_2O_4$ (ppm)	H_2 (LPM)	Load (%)	BTE (%)	BSEC (MJ kW^{-1} h^{-1})	NO_x (ppm)	Smoke (FSN)	CO (%)	HC (ppm)	BTE × BSEC
75	5	100	32.12	6.723	978	4.38	0.049	13.8	215.94
150	8	100	33.51	6.440	1055	4.18	0.047	12.5	215.80
200	5	100	33.84	6.380	1028	4.12	0.046	12.2	215.90
150	5	120[a]	33.65	6.410	1080	4.15	0.047	12.4	215.70
0	10	100	29.80	7.248	1010	4.65	0.048	14.1	215.99

[a] Hypothetical overload condition used to probe model behaviour.

Table 6 Experimental validation of PE-MTMML predictions at untested intermediate condition ($NiFe_2O_4$ 75 ppm + H_2 5 LPM at 100% load)

Parameter	Experimental	PE-MTMML predicted	Absolute error	Relative error (%)
BTE (%)	32.28	32.12	0.16	0.50
BSEC (MJ kW^{-1} h^{-1})	6.76	6.723	0.037	0.55
NO_x (ppm)	992	978	14	1.43
Smoke (FSN)	4.42	4.38	0.04	0.91
CO (%)	0.0483	0.049	0.0007	1.43
HC (ppm)	14.2	13.8	0.4	2.9

not included in the training set, as presented in Table 5. These predictions were subsequently validated experimentally for one critical intermediate condition, demonstrating the model's capability to accurately predict performance at untested nanoparticle dosages. It is important to distinguish these results from the validation set; while Table 4 confirms predictive accuracy through direct experimental comparison, Table 5 demonstrates the model's ability to maintain physical consistency in unmapped regimes. The PE-MTMML's ultimate value resides in its capability to forecast performance and emissions with high reliability outside the restricted experimental matrix while strictly adhering to the laws of physics, a fundamental requirement for actual engine development where extensive testing is unacceptably costly and time-consuming. To the best of our knowledge, this type of physics-constrained extrapolation for nanoparticle-enriched biodiesel systems has not been reported in previous literature.

The performance of the model in predicting the behaviour of the system under the most extreme operating conditions not included in the training set is shown in Table 5. The harshest conditions found were the very high dosages of nanoparticles (200 ppm), high H_2 flow rates (10 LPM), and over-load situations assumed (120% load). This hypothetical overload condition was specifically included to probe the model's stability; unlike standard data-driven models which often predict erratic values outside the training range, the PE-MTMML framework maintained thermodynamic consistency even in this extreme, unmapped regime. Under these conditions the model still provided flawless, physically possible predictions: even a little bit more efficient BTE (~1–2% but negligible), no more smoke, CO, and HC, and a controlled expansion of NO_x which is still within the limits tolerable for the latest after-treatment systems. Most importantly, the thermodynamic constraint BTE × BSEC has been satisfied with an error of max. 0.005% in all situations.

This strong generalization is a direct consequence of the physics-encoded architecture: Non-physical outputs are intrinsically guarded by the thermodynamic and emission-restriction constraints which effectively expand the domain of reliable predictions far beyond the 25 measured points. The trained model can, in practical terms, be used on an engine control unit (ECU) or digital-twin platform for real-time optimization of nanoparticle dosing and H_2 enrichment, thus allowing adaptive tri-fuel strategies that enhance efficiency and decrease carbon emissions while maintaining NO_x within legal limits by means of mild EGR or injection-timing alterations.

Table 6 presents a comprehensive comparison between experimental measurements and PE-MTMML predictions for this validation condition. The model demonstrated exceptional accuracy across all six output parameters, with prediction errors ranging from 0.50% to 2.90%. Critically, all errors fall well within the experimental uncertainty bounds, confirming that the observed discrepancies are attributable to normal measurement variability rather than systematic model inadequacy.

Essentially, by cutting the requirement for expensive iterative experiments by over 90%, the PE-MTMML framework is the main reason for how fast the described technological chain can be changed to produce a genuinely carbon-superior alternative to fossil diesel in stationary power generation, marine, and heavy-duty transport applications. This waste-cooking-oil-derived biodiesel is augmented with low-cost $NiFe_2O_4$ nanocatalysts and modest H_2 fumigation. The method disclosed here can be used for any other oxygenated biofuels, metal-oxide additives, and low-carbon e-fuels, thus providing a scalable route to net-zero combustion engines.

5 Conclusion

This research assessed the use of a tri-fuel strategy by mixing WCOB, $NiFe_2O_4$ nanocatalysts, and H_2 enrichment in a single-cylinder diesel engine, aided by a PE-MTMML model. The

combined experimental and computational approach revealed that catalytic enhancement and reactive fuel supplementation are two effective ways to eliminate the intrinsic limitations of biodiesel, thus, improving combustion behavior, increasing thermal efficiency, and reducing exhaust emissions.

The experimental results confirmed well-known trends reported in recent literature,[28] demonstrating that significant improvements were made in the main performance and combustion metrics. Under full load, the WCOB + $NiFe_2O_4$ 150 ppm + H_2 blend raised peak cylinder pressure by 7.8% and heat release rate by 12–14% in comparison with diesel. BTE was raised by 29.2% over WCOB and 15.4% over diesel, whereas BSEC was lowered by 22.3% with respect to diesel. The smoke opacity, CO, and HC were reduced by 10.9%, 20%, and 25%, respectively, while NO_x was increased slightly by 7.5% due to enhanced premixed combustion. The PE-MTMML model attained outstanding precision (mean $R^2 = 0.9993$) and closely followed thermodynamic constraints, thus confirming its role as a high-fidelity predictive tool.

Crucially, this study highlights that the PE-MTMML framework succeeds where conventional ML often struggles by embedding physical laws (thermodynamic reciprocity and emission formation mechanisms) directly into the loss function. This physics-encoding was the key factor enabling the model to simulate the complex non-linear interactions of the biodiesel-nanoparticle-H_2 system with high fidelity, even with a limited dataset. In contrast to previous ML applications in engine research that rely solely on large historical datasets, this approach demonstrates that incorporating domain knowledge allows for accurate generalization in novel, data-sparse systems like the specific tri-fuel engine reported here.

A comparative analysis highlighted the distinct advantage of this physics-encoded framework over purely experimental observation. Positively, the model and experiments showed excellent agreement on the synergistic effects of H_2 and nanoparticles on thermal efficiency and emissions reduction. Conversely, the model succeeded where experimentation reached its limits: while raw experimental data exhibited stochastic noise and minor deviations from energy balance (particularly at low loads), the PE-MTMML model successfully filtered these artifacts to reveal the strict thermodynamic reciprocity (BTE $\times$ BSEC $\approx$ constant) governing the system. This effectively allowed the detection of physical truths that were obscured by measurement uncertainty in the experimental phase.

The results lead to the conclusion that the synergistic effect of $NiFe_2O_4$ nanocatalysis and H_2 enrichment is the main reason why WCOB is a high-efficiency, low-emission fuel for compression-ignition engines. The tri-fuel strategy suggested not only creates the conditions for carbon-neutral engine operation but also the physics-encoded machine learning framework acts as a dependable digital twin for performance optimization, emissions control, and quick adaptation of the next generation of sustainable combustion systems. Specifically, the PE-MTMML model represents a significant step forward in alternative-fuel engine modeling. It is one of the very few machine learning frameworks to directly combine thermodynamic equations and emission chemistry within a multi-task structure for biodiesel-nanoparticle-H_2 systems. The imposition of the physics-based constraints allows the model to generalize better than classical approaches like ANN or SVM, while its multi-task capability eliminates computational redundancy. Thus, this application presents a powerful analytical tool for the optimization of low-carbon fuels led by nanocatalyst-assisted H_2-enriched diesel engine strategies.

6 Future research

Research beyond should first optimize nanoparticle formulations $NiFe_2O_4$, such as hybrid or doped ferrites, and fine-tune H_2 enrichment *via* load-adaptive or closed-loop control strategies. Along with advanced optical diagnostics to reveal spray–flame evolution and catalytic oxidation mechanisms, it is vital to measure engine durability over the very long term, health of the injector, and nanoparticle lubricant interactions. To offset the improvements in efficiency with NO_x abatement, the use of exhaust gas recirculation, water injection, and after-treatment systems needs to be combined. It is important to scale up multi-cylinder engines, carry out real-cycle testing, and conduct thorough life cycle and techno-economic analyses to figure out industrial feasibility. Besides that, advanced physics-encoded artificial intelligence models with multi-zone combustion physics and transient training data can be a great help in real-time optimization and the use of adaptive tri-fuel engine systems.

Conflicts of interest

There are no conflicts to declare.

Data availability

The data that supports the findings of this study are available within the article.

Supplementary information (SI): the experimental procedure and uncertainty analysis. See DOI: https://doi.org/10.1039/d5ra09336h.

References

1 H. K. Jeswani, A. Chilvers and A. Azapagic, Environmental sustainability of biofuels: A review: Environmental sustainability of biofuels, *Proc. R. Soc. A*, 2020, **476**, 20200351, DOI: 10.1098/RSPA.2020.0351.

2 C. G. Lopresto, Sustainable biodiesel production from waste cooking oils for energetically independent small communities: an overview, *Int. J. Environ. Sci. Technol.*, 2025, **22**, 1953–1974, DOI: 10.1007/S13762-024-05779-2.

3 S. Bhangwar, A. M. Liaquat, M. R. Luhar, A. Abbasi, L. Kumar, U. A. Rajput, *et al.*, Production of biodiesel and analysis of exhaust particulate emissions and metal concentration of lubricant oil of the compression ignition engine, *Front. Energy Res.*, 2022, **10**, 1057611, DOI: 10.3389/FENRG.2022.1057611/FULL.

4 D. Christopher Selvam and Y. Devarajan, Performance and emission analysis of sterculia foetida biodiesel enhanced with butanol: Combustion efficiency and emission mitigation, *Results Eng.*, 2025, **25**, 104586, DOI: 10.1016/j.rineng.2025.104586.
5 D. Christopher Selvam and Y. Devarajan, Evaluating the performance, combustion, and emission characteristics of decanol-enhanced sterculia foetida biodiesel in diesel engines, *Results Eng.*, 2025, **26**, 104936, DOI: 10.1016/j.rineng.2025.104936.
6 E. P. Venkatesan, R. Krishnaiah, K. Prasad, S. R. Medapati, S. R. Sree, M. Asif, *et al.*, Compatibility Effects of Waste Cooking Oil Biodiesel Blend on Fuel System Elastomers in Compression Ignition Engines, *ACS Omega*, 2024, **9**, 6709–6718, DOI: 10.1021/ACSOMEGA.3C07871.
7 Y. Devarajan and D. Christopher Selvam, Utilization of sterculia foetida oil as a sustainable feedstock for biodiesel production: optimization, performance, and emission analysis, *Results Eng.*, 2024, **24**, 103196, DOI: 10.1016/j.rineng.2024.103196.
8 R. K. Gaur and R. Goyal, Performance, emission, combustion and economics analysis of CI engine fueled with mixed oil biodiesel blends from waste cooking oil and pongamia oil, *Discov. Appl. Sci.*, 2025, **7**(6), DOI: 10.1007/S42452-025-07150-7.
9 S. T. Jeur, K. A. Sorate and P. V. Bhale, Energy-efficient biodiesel production via hydrodynamic cavitation: Comparative study of soybean and waste cooking oil, *Energy Convers. Manag.*, 2026, **348**, 120577, DOI: 10.1016/j.enconman.2025.120577.
10 D. Beyene, D. Bekele, B. Abera, D. Beyene, D. Bekele and B. Abera, Biodiesel from blended microalgae and waste cooking oils: Optimization, characterization, and fuel quality studies, *AIMS Energy*, 2024, (12), 408–438, DOI: 10.3934/ENERGY.2024019.
11 D. Beyene, D. Bekele and B. Abera, Biodiesel from blended microalgae and waste cooking oils: Optimization, characterization, and fuel quality studies, *AIMS Energy*, 2024, **12**, 408–438, DOI: 10.3934/ENERGY.2024019.
12 M. Sonachalam, V. Manieniyan, R. Senthilkumar, R. M. K, M. Warimani, R. Kumar, *et al.*, Experimental investigation of performance, emission, and combustion characteristics of a diesel engine using blends of waste cooking oil-ethanol biodiesel with MWCNT nanoparticles, *Case Stud. Therm. Eng.*, 2024, **61**, 105094, DOI: 10.1016/J.CSITE.2024.105094.
13 S. Debbarma, R. D. Misra and B. Das, Performance of graphene-added palm biodiesel in a diesel engine, *Clean Technol. Environ. Policy*, 2020, **22**, 523–534, DOI: 10.1007/s10098-019-01800-2.
14 J. Liu, X. Zhang, C. Tang, L. Wang, P. Sun and P. Wang, Effects of palm oil biodiesel addition on exhaust emissions and particle physicochemical characteristics of a common-rail diesel engine, *Fuel Process. Technol.*, 2023, **241**, 107606, DOI: 10.1016/j.fuproc.2022.107606.
15 D. T. Luong and V. P. Vu, A comparative study on the effect of nano-additives on the performance and emissions of a diesel engine run on palm biodiesel, *Nanotechnol. Environ. Eng.*, 2024, **9**, 519–523, DOI: 10.1007/S41204-024-00381-W.
16 A. I. EL-Seesy, H. Hassan and S. Ookawara, Performance, combustion, and emission characteristics of a diesel engine fueled with Jatropha methyl ester and graphene oxide additives, *Energy Convers. Manag.*, 2018, **166**, 674–686, DOI: 10.1016/j.enconman.2018.04.049.
17 E. Ramachandran, R. Krishnaiah, E. P. Venkatesan, S. Shaik, C. A. Saleel and F. Hussain, Investigation into the Ideal Concoction for Performance and Emissions Enhancement of Jatropha Biodiesel-Diesel with CuO Nanoparticles Using Response Surface Methodology, *ACS Omega*, 2023, **8**, 39067–39079, DOI: 10.1021/ACSOMEGA.3C03890.
18 E. Ramachandran, R. Krishnaiah, E. P. Venkatesan, S. Shaik, C. A. Saleel and F. Hussain, Investigation into the Ideal Concoction for Performance and Emissions Enhancement of Jatropha Biodiesel-Diesel with CuO Nanoparticles Using Response Surface Methodology, *ACS Omega*, 2023, **8**, 39067–39079, DOI: 10.1021/ACSOMEGA.3C03890.
19 B. R. Varpe and Y. R. Kharde, Combined effect of DEE and Jatropha biodiesel–diesel fuel blends on the enhancement of VCR diesel engine parameters at varying loads and compression ratios, *Aust. J. Mech. Eng.*, 2023, **21**, 1843–1860, DOI: 10.1080/14484846.2022.2038405.
20 P. Moonsin, W. Roschat, S. Phewphong, S. Watthanalao, B. Maneerat, A. Thammayod, *et al.*, Development of liquid biofuel properties through the blending of biodiesel from used cooking oil and pyrolysis oil from low-quality rubber waste, *Case Stud. Chem. Environ. Eng.*, 2025, **11**, 101230, DOI: 10.1016/j.cscee.2025.101230.
21 P. V. Elumalai, M. Parthasarathy, V. Hariharan, J. Jayakar and S. Mohammed Iqbal, Evaluation of water emulsion in biodiesel for engine performance and emission characteristics, *J. Therm. Anal. Calorim.*, 2022, **147**, 4285–4301, DOI: 10.1007/S10973-021-10825-Z.
22 H. A. Dhahad, S. A. Ali and M. T. Chaichan, Combustion analysis and performance characteristics of compression ignition engines with diesel fuel supplemented with nano-TiO2 and nano-Al2O3, *Case Stud. Therm. Eng.*, 2020, **20**, 100651, DOI: 10.1016/j.csite.2020.100651.
23 D. Christopher Selvam and Y. Devarajan, Bio-inspired hybrid materials for sustainable energy: Advancing bioresource technology and efficiency, *Mater. Today Commun.*, 2025, **46**, 112647, DOI: 10.1016/j.mtcomm.2025.112647.
24 S. D. Prasetyo, E. P. Budiana, A. R. Prabowo and Z. Arifin, Modeling Finned Thermal Collector Construction Nanofluid-based Al2O3 to Enhance Photovoltaic Performance, *J. Civ. Eng.*, 2023, **9**, 2989–3007, DOI: 10.28991/CEJ-2023-09-12-03.
25 C. L. Sung, R. H. Wang, Y. C. Shih, Z. Y. Wu, S. R. Alvarado, Y. H. Chang, *et al.*, g-C3N4 Nanosheet Supported CuO Nanocomposites for the Electrochemical Carbon Dioxide

Reduction Reaction, *ACS Omega*, 2023, **8**, 7368–7377, DOI: 10.1021/ACSOMEGA.2C05513.

26 A. F. Chen, A. M. Akmal, A. Adam, M. F. Othman, M. K. Kamaruzzaman and A. G. Mrwan, Combustion characteristics, engine performances and emissions of a diesel engine using nanoparticle-diesel fuel blends with aluminium oxide, carbon nanotubes and silicon oxide, *Energy Convers. Manag.*, 2018, **171**, 461–477, DOI: 10.1016/j.enconman.2018.06.004.

27 J. Y. Ma, H. Zhao, R. R. Mercer, M. Barger, M. Rao, T. Meighan, *et al.*, Cerium oxide nanoparticle-induced pulmonary inflammation and alveolar macrophage functional change in rats, *Nanotoxicology*, 2011, **5**, 312–325, DOI: 10.3109/17435390.2010.519835.

28 G. M. L. Leo, G. Thodda and S. Murugapoopathi, Experimental investigation on effects of gasoline premixed - Al2O3 additive blended fish oil biodiesel fuelled HCCI-DI engine, *J. Phys., Conf. Ser.*, 2021, **2054**, 012040, DOI: 10.1088/1742-6596/2054/1/012040.

29 Z. Li, D. Liao, G. Tian, X. Fan, X. Chai, W. Chang, Y. Gao, B. Yuan, Z. Li, F. Wei and C. Zhang, Determination of Mn Valence States in Nanocatalysts During Sustainable Syngas Conversion, *J. Am. Chem. Soc.*, 2025, **147**(36), 32548–32559, DOI: 10.1021/jacs.5c06550.

30 F. Bazdidi-Tehrani, E. Sharifi-Sedeh and M. S. Abedinejad, Effects of alumina nanoparticles on evaporation and combustion characteristics of diesel fuel droplets, *J. Taiwan Inst. Chem. Eng.*, 2023, **143**, 104713, DOI: 10.1016/j.jtice.2023.104713.

31 N. S. Kiran, H. Paliwal, C. Yashaswini, S. Singh, B. G. Prajapati and A. Chatterjee, Biogenic Metallic Nanoparticles from Waste Biomass: Advances in Green Synthesis, Characterization, and Multifunctional Applications, *Waste Biomass Valoriz.*, 2025, **16**(9), 4605–4628, DOI: 10.1007/S12649-025-03280-6.

32 B. Tegze, G. Tolnai, D. Hessz, M. Kubinyi, J. Madarász, G. Sáfrán, *et al.*, Effect of heat treatment temperature on the morphology and upconversion properties of LaF3:Yb,Er nanoparticles, *J. Therm. Anal. Calorim.*, 2023, **148**, 10795–10802, DOI: 10.1007/S10973-023-12417-5.

33 K. Tiwari, K. Biswas. *In-Situ Transmission Electron Microscopy Investigation of Phase Transformation Behavior of Alloy Nanoparticles* 2022:103–116. doi: DOI: 10.1007/978-981-16-5101-4_8.

34 K. Srinivasa Reddy, H. R. Y. Venkata and V. Dhana Raju, Experimental assessment of copper oxide nanoparticles on the attributes of diesel engines fuelled with waste plastic biodiesel, *Int. J. Ambient Energy*, 2024, **45**(1), DOI: 10.1080/01430750.2024.2307414.

35 S. Li, Q. Yang, L. Ye, H. Du, Z. Zhang, X. Huang, *et al.*, Effect of Nanoparticle Concentration on Physical and Heat-Transfer Properties and Evaporation Characteristics of Graphite/n-Decane Nanofluid Fuels, *ACS Omega*, 2022, **7**, 3284–3292, DOI: 10.1021/ACSOMEGA.1C05343.

36 Y. Yang, M. Ma, L. Li, S. Chen, Z. Liu, F. Li, *et al.*, Formation characteristics of soot from the combustion of biodiesel-based nanofluid fuel: Influence of non-metallic nanoparticles, *Fuel*, 2025, **399**, 135484, DOI: 10.1016/j.fuel.2025.135484.

37 D. Firew, G. Alemayehu, R. B. Nallamothu, S. K. Kang. Effect of Nanoparticles on the Performance and Emission Characteristics of Diesel Engine Operated with Different Fuels. *Lecture Notes in Mechanical Engineering* 2021:279–291. doi: DOI: 10.1007/978-981-16-0976-3_27.

38 M. Mofijur, S. F. Ahmed, B. Ahmed, T. Mehnaz, F. Mehejabin, S. Shome, *et al.*, Impact of nanoparticle-based fuel additives on biodiesel combustion: An analysis of fuel properties, engine performance, emissions, and combustion characteristics, *Energy Convers. Manag.*, 2024, **21**, 100515, DOI: 10.1016/j.ecmx.2023.100515.

39 K. N. Krishnamurthy, B. S. Ajith, V. Birur Jayanna, G. C. M. Patel and S. Sarıkoç, Nanoparticles in Biodiesel Production and Engine Use: A Path toward Sustainable and Eco-Friendly, *Fuel*, 2026, 371–420, DOI: 10.1007/978-3-031-94536-6_29.

40 A. Bin Rashid and Y. Hayashi, Utilization of Nanotechnology and Nanomaterials in Biodiesel Production and Property Enhancement, *J. Nanomater.*, 2023, **2023**, 1–14, DOI: 10.1155/2023/7054045.

41 K. N. Krishnamurthy, B. S. Ajith, V. Birur Jayanna, G. C. M. Patel and S. Sarıkoç, Nanoparticles in Biodiesel Production and Engine Use: A Path toward Sustainable and Eco-Friendly, *Fuel*, 2026, 371–420, DOI: 10.1007/978-3-031-94536-6_29.

42 D. Balasubramanian, J. R. S. Gnanavel, I. P. Venugopal and H. W. Wu, Enhanced Combustion Characteristics of Diesel, Biodiesel Blends Infused with Cobalt Oxide Nanoparticles: Droplet-Scale Experimentation and Flame Analysis, *Combust. Sci. Technol.*, 2025, 1–44, DOI: 10.1080/00102202.2025.2509246.

43 C. Jin, J. Wei, B. Chen, X. Li, D. Ying, L. Gong, *et al.*, Effect of nanoparticles on diesel engines driven by biodiesel and its blends: A review of 10 years of research, *Energy Convers. Manag.*, 2023, **291**, 117276, DOI: 10.1016/j.enconman.2023.117276.

44 A. A. Yusuf, H. Dandakouta, I. Yahuza, D. A. Yusuf, M. A. Mujtaba, A. S. El-Shafay, *et al.*, Effect of low CeO2 nanoparticles dosage in biodiesel-blends on combustion parameters and toxic pollutants from common-rail diesel engine, *Atmos. Pollut. Res.*, 2022, **13**, 101305, DOI: 10.1016/j.apr.2021.101305.

45 B. M. Reddy and A. Khan, Nanosized CeO2-SiO2, CeO2-TiO2, and CeO2-ZrO2 mixed oxides: Influence of supporting oxide on thermal stability and oxygen storage properties of ceria, *Catal. Surv. Asia*, 2005, **9**, 155–171, DOI: 10.1007/S10563-005-7552-1.

46 B. Chetia, S. Debbarma and B. Das, Enhancing engine performance, combustion, and emissions characteristics through CeO2-modified cottonseed biodiesel with hydrogen enrichment: A comprehensive investigation, *Int. J. Hydrogen Energy*, 2024, **89**, 1149–1165, DOI: 10.1016/j.ijhydene.2024.09.417.

47 K. Polychronopoulou, A. A. Alkhoori, A. M. Efstathiou, M. A. Jaoude, C. M. Damaskinos, M. A. Baker, *et al.*,

Design Aspects of Doped CeO2for Low-Temperature Catalytic CO Oxidation: Transient Kinetics and DFT Approach, *ACS Appl. Mater. Interfaces*, 2021, **13**, 22391–22415, DOI: 10.1021/ACSAMI.1C02934.

48 R. Sabarish, S. Jenoris Muthiya, B. Anandan, D. Sathis Kumar, B. Manideep, P. Sekar, *et al.*, The Role and Impact of Al2O3 Additive on the Performance of the Diesel Engine Operated by JFO Along With Its Measures of Combustion and Emissions, *Energy Sci. Eng.*, 2025, **13**, 995–1010, DOI: 10.1002/ESE3.2064.

49 A. Dave and S. N. Reddy, Solvothermal liquefaction of Tetra Pak waste into biofuels and Al2O3-carbon nanocomposite, *Waste Manage.*, 2023, **171**, 642–652, DOI: 10.1016/j.wasman.2023.10.013.

50 P. Promhuad, B. Sawatmongkhon, K. Theinnoi, T. Wongchang, N. Chollacoop, E. Sukjit, *et al.*, Effect of Metal Oxides (CeO2, ZnO, TiO2, and Al2O3) as the Support for Silver-Supported Catalysts on the Catalytic Oxidation of Diesel Particulate Matter, *ACS Omega*, 2024, **9**, 19282–19294, DOI: 10.1021/ACSOMEGA.4C00218.

51 P. Promhuad, B. Sawatmongkhon, K. Theinnoi, T. Wongchang, N. Chollacoop, E. Sukjit, *et al.*, Effect of Metal Oxides (CeO2, ZnO, TiO2, and Al2O3) as the Support for Silver-Supported Catalysts on the Catalytic Oxidation of Diesel Particulate Matter, *ACS Omega*, 2024, **9**, 19282–19294, DOI: 10.1021/ACSOMEGA.4C00218.

52 A. Calam, R. Ali, H. Solmaz and H. S. Yücesu, An experimental evaluation of TiO2 nanoadditive for HCCI engines running on ABE fuel, *Energy*, 2024, **313**, 133837, DOI: 10.1016/J.ENERGY.2024.133837.

53 S. Vijayan, R. Sathyamurthy, E. M. A. Mokheimer and R. S. Kumar, Performance enhancement and emission reduction of CRDI diesel engine fueled using Manilkara Zapota biodiesel blend with TiO2 nanoadditive, *Fuel Process. Technol.*, 2023, **248**, 107842, DOI: 10.1016/J.FUPROC.2023.107842.

54 J. Singh, M. Srivastava, P. Kalita and B. D. Malhotra, A novel ternary NiFe2O4/CuO/FeO-chitosan nanocomposite as a cholesterol biosensor, *Process Biochem.*, 2012, **47**, 2189–2198, DOI: 10.1016/j.procbio.2012.08.012.

55 Ö. N. Avcl, L. Sementa and A. Fortunelli, Mechanisms of the Oxygen Evolution Reaction on NiFe2O4and CoFe2O4Inverse-Spinel Oxides, *ACS Catal.*, 2022, **12**, 9058–9073, DOI: 10.1021/ACSCATAL.2C01534.

56 M. Saberi, S. S. A. Talesh and B. Maleki, Biodiesel production from waste frying oil via NiFe2O4/SiO2 magnetic nanocomposites: Evaluation of diesel engine parameters and statistical optimization, *Renew. Energy*, 2025, **254**, 123727, DOI: 10.1016/j.renene.2025.123727.

57 R. M. Kalil, S. Santhoshkumar, D. Subramaniam, A. Avinash and A. Pugazhendhi, Effects of oxygenated fuel pertaining to fuel analysis on diesel engine combustion and emission characteristics, *Energy*, 2022, **239**, 122373, DOI: 10.1016/j.energy.2021.122373.

58 L. Fleitmann, P. Ackermann, J. Schilling, J. Kleinekorte, J. G. Rittig, F. vom Lehn, *et al.*, Molecular Design of Fuels for Maximum Spark-Ignition Engine Efficiency by Combining Predictive Thermodynamics and Machine Learning, *Energy Fuels*, 2023, **37**, 2213–2229, DOI: 10.1021/ACS.ENERGYFUELS.2C03296.

59 N. S. Sarvestani, M. H. Abbaspour Fard, M. Tabasizadeh, H. Nayebzadeh, P. Arora, P. Verma, *et al.*, Synthesis and evaluation of catalytic activity of NiFe2O4 nanoparticles in a diesel engine: An experimental investigation and Multi-Criteria Decision Making approach, *J. Clean. Prod.*, 2022, **365**, 132818, DOI: 10.1016/j.jclepro.2022.132818.

60 M. Kooti and A. N. Sedeh, Synthesis and Characterization of NiFe2O4 Magnetic Nanoparticles by Combustion Method, *J. Mater. Sci. Technol.*, 2013, **29**, 34–38, DOI: 10.1016/j.jmst.2012.11.016.

61 H. Liao, F. Hu, X. Wu, P. Li, C. Ding, C. Yang, *et al.*, Effects of H2 addition on the characteristics of the reaction zone and NOx mechanisms in MILD combustion of H2-rich fuels, *Int. J. Hydrogen Energy*, 2024, **58**, 174–189, DOI: 10.1016/j.ijhydene.2024.01.154.

62 V. C. Pham, V. V. Le, V. S. Hoang, W. J. Lee, S. Choe and J. H. Choi, Cutting carbon emissions by using H2 gas on a heavy-duty 2-stroke marine engine, *J. Int. Marit. Saf. Environ. Aff. Shipp.*, 2025, **9**, 2476847, DOI: 10.1080/25725084.2025.2476847.

63 H. A. Mahmood, Mariah, N. Adam, B. B. Sahari and S. U. Masuri, Development of a particle swarm optimisation model for estimating the homogeneity of a mixture inside a newly designed CNG-H2-AIR mixer for a dual fuel engine: An experimental and theoretic study, *Fuel*, 2018, **217**, 131–150, DOI: 10.1016/J.FUEL.2017.12.066.

64 M. U. S. Akhtar, F. Asfand, A. S. Mishamandani, R. Mishra and M. I. Khan, Hydrogen as a sustainable combustion fuel: Performance, challenges, and pathways for transition to low-carbon propulsion systems, *Renew. Sustain. Energy Rev.*, 2025, **223**, 116004, DOI: 10.1016/j.rser.2025.116004.

65 H. Q. Do, A. Faccinetto, L. S. Tran, P. Desgroux, L. Gasnot, A. El Bakali, *et al.*, Hydrogen as a fuel additive in laminar premixed methane flames: Impact on the nucleation and growth of soot particles, *Fuel*, 2022, **315**, 123125, DOI: 10.1016/j.fuel.2021.123125.

66 M. Zhang, M. Chang, J. Wang and Z. Huang, Flame dynamics analysis of highly hydrogen-enrichment premixed turbulent combustion, *Int. J. Hydrogen Energy*, 2020, **45**, 1072–1083, DOI: 10.1016/j.ijhydene.2019.10.194.

67 M. A. K. Nzinga, A. M. Dall, M. E. P. Pintos and A. Z. Mendiburu, Experimental Observation of Flame Propagation Behavior of Hydrogen Enriched Flames Upstream of a Flame Arrester Housing with Parallel Plates as the Arrester Element, *Combust. Sci. Technol.*, 2025, **197**, 2036–2059, DOI: 10.1080/00102202.2024.2302366.

68 P. S. Varma and M. Mittal, Experimental and numerical investigations to study the effects of hydrogen enrichment on a retrofitted CNG SI engine operating at a low load condition, *Fuel*, 2025, **392**, 134914, DOI: 10.1016/j.fuel.2025.134914.

69 L. Liu, Z. Xu, L. Wang, Y. Wang, H. Li and Y. Wu, Theoretical analysis on high-efficiency combustion and emissions reduction strategy of ammonia-diesel direct

injection marine medium-speed engines under energizing-intensifying composite combustion mode, *Appl. Therm. Eng.*, 2025, **278**, 127391, DOI: 10.1016/j.applthermaleng.2025.127391.

70 M. R. Atelge, Experimental study of a blend of Diesel/Ethanol/n-Butanol with hydrogen additive on combustion and emission and exegetic evaluation, *Fuel*, 2022, **325**, 124903, DOI: 10.1016/j.fuel.2022.124903.

71 N. Mohanrajhu, G. Magudeeswaran, R. Jayabal and P. Prabakar, Experimental assessment of sustainable multi-fuel strategies: Algal biodiesel, bioethanol, graphene oxide nanoparticles, and hydrogen fumigation in diesel engine applications, *Environ. Prog. Sustain. Energy*, 2025, e70243, DOI: 10.1002/ep.70243.

72 A. Madhan Kumar, K. Senthil Nathan, S. Manickam, D. Gupta, M. Vikneswaran, G. Dhamodaran, *et al.*, Effect of TiO2 nanoparticles and hydrogen on the combustion, performance, and emissions of madhuca biodiesel in a diesel engine, *Int. J. Hydrogen Energy*, 2025, **143**, 635–649, DOI: 10.1016/j.ijhydene.2025.04.312.

73 B. Chetia, S. Debbarma and B. Das, An experimental investigation of hydrogen-enriched and nanoparticle blended waste cooking biodiesel on diesel engine, *Int. J. Hydrogen Energy*, 2024, **49**, 23–37, DOI: 10.1016/j.ijhydene.2023.06.088.

74 O. Khan, M. Z. Khan, B. K. Bhatt, M. T. Alam and M. Tripathi, Multi-objective optimization of diesel engine performance, vibration and emission parameters employing blends of biodiesel, hydrogen and cerium oxide nanoparticles with the aid of response surface methodology approach, *Int. J. Hydrogen Energy*, 2023, **48**, 21513–21529, DOI: 10.1016/j.ijhydene.2022.04.044.

75 O. Khan, I. Alsaduni, M. Parvez, Z. Yahya and A. K. Yadav, Role of hydrogen-enrichment on performance and emission characteristics of a diesel engine fuelled with metal oxide nanoparticles added biodiesel/diesel blends:A combined neuro Fuzzy-Gaussian Mixture Model analysis, *Int. J. Hydrogen Energy*, 2024, **93**, 1113–1126, DOI: 10.1016/j.ijhydene.2024.11.032.

76 O. Khan, V. Ali, M. Parvez, A. Alhodaib, Z. Yahya, A. K. Yadav, *et al.*, Exploring the performance of biodiesel-hydrogen blends with diverse nanoparticles in diesel engine: A hybrid machine learning K-means clustering approach with weighted performance metrics, *Int. J. Hydrogen Energy*, 2024, **78**, 547–563, DOI: 10.1016/j.ijhydene.2024.06.303.

77 E. N. Tec-Caamal, S. K. Kamarudin and A. Pugazhendhi, Synergistic effects of CeO2 nanoparticles and HHO gas on biodiesel blends in CI engine performance and emissions, *Int. J. Hydrogen Energy*, 2025, **143**, 691–700, DOI: 10.1016/j.ijhydene.2025.04.449.

78 A. Z. Hameed and K. Muralidharan, Performance, Emission, and Catalytic Activity Analysis of AL2O3 and CEO2 Nano-Additives on Diesel Engines Using Mahua Biofuel for a Sustainable Environment, *ACS Omega*, 2023, **8**, 5692–5701, DOI: 10.1021/ACSOMEGA.2C07193.

79 R. Kumar, M. Arunkumar, D. P. Shan, P. P. Patil, R. Kumar, B. Singh, *et al.*, Performance and Emission Analysis of Waste Cooking Oil Biodiesel Mixed with Titanium Oxide Nano-Additives, *Int. J. Chem. Eng.*, 2022, **2022**, 1101771, DOI: 10.1155/2022/1101771.

80 M. Mofijur, S. F. Ahmed, B. Ahmed, T. Mehnaz, F. Mehejabin, S. Shome, *et al.*, Impact of nanoparticle-based fuel additives on biodiesel combustion: An analysis of fuel properties, engine performance, emissions, and combustion characteristics, *Energy Convers. Manag.*, 2024, **21**, 100515, DOI: 10.1016/j.ecmx.2023.100515.

81 O. Khan, V. Ali, M. Parvez, A. Alhodaib, Z. Yahya, A. K. Yadav, *et al.*, Exploring the performance of biodiesel-hydrogen blends with diverse nanoparticles in diesel engine: A hybrid machine learning K-means clustering approach with weighted performance metrics, *Int. J. Hydrogen Energy*, 2024, **78**, 547–563, DOI: 10.1016/j.ijhydene.2024.06.303.

82 M. U. S. Akhtar, F. Asfand, A. S. Mishamandani, R. Mishra and M. I. Khan, Hydrogen as a sustainable combustion fuel: Performance, challenges, and pathways for transition to low-carbon propulsion systems, *Renew. Sustain. Energy Rev.*, 2025, **223**, 116004, DOI: 10.1016/j.rser.2025.116004.

83 S. Sanyasi Rao, J. Paparao, M. V. J. Raju and S. Kumar, Effect of nanoparticle-doped biofuel in a dual-fuel diesel engine with oxy-hydrogen gas, *Int. J. Hydrogen Energy*, 2024, **70**, 146–158, DOI: 10.1016/j.ijhydene.2024.05.131.

84 B. Chetia, S. Debbarma and B. Das, An experimental investigation of hydrogen-enriched and nanoparticle blended waste cooking biodiesel on diesel engine, *Int. J. Hydrogen Energy*, 2024, **49**, 23–37, DOI: 10.1016/j.ijhydene.2023.06.088.

85 E. N. Tec-Caamal, S. K. Kamarudin and A. Pugazhendhi, Synergistic effects of CeO2 nanoparticles and HHO gas on biodiesel blends in CI engine performance and emissions, *Int. J. Hydrogen Energy*, 2025, **143**, 691–700, DOI: 10.1016/j.ijhydene.2025.04.449.

86 N. Mohanrajhu, G. Magudeeswaran, R. Jayabal and P. Prabakar, Experimental assessment of sustainable multi-fuel strategies: Algal biodiesel, bioethanol, graphene oxide nanoparticles, and hydrogen fumigation in diesel engine applications, *Environ. Prog. Sustain. Energy*, 2025, e70243, DOI: 10.1002/EP.70243.

87 C. Rekatsinas, P. Krokidas, V. Vavourakis, C. Essmann and G. Giannakopoulos, A Physics Constrained Machine Learning Pipeline for Young's Modulus Prediction in Multimaterial Hyperelastic Cylinders Guided by Contact Mechanics, *Adv. Intell. Syst.*, 2025, 202500092, DOI: 10.1002/aidi.202500092.

88 S. Cuomo, V. S. Di Cola, F. Giampaolo, G. Rozza, M. Raissi and F. Piccialli, Scientific Machine Learning Through Physics–Informed Neural Networks: Where we are and What's Next, *Comput. Sci. J.*, 2022, **92**, 88, DOI: 10.1007/s10915-022-01939-z.

89 X. Chen, K. Fan, C. Wang, S. Wu, R. Zheng, X. Mi, *et al.*, Predicting high-yield tight gas sweet spots in the Qiulin

area, Sichuan Basin, *J. Earth Syst. Sci.*, 2025, **134**, 81, DOI: 10.1007/s12040-025-02544-y.

90 M. Tajabadi Ebrahimi and M. Fakoor, Multidisciplinary approaches to microstructural impacts on strength and fracture: from fundamental equations to machine learning techniques, *Appl. Phys. A: Mater. Sci. Process.*, 2025, **131**(9), DOI: 10.1007/s00339-025-08804-4.

91 A. I. Osman, M. Nasr, M. Farghali, A. K. Rashwan, A. Abdelkader, A. H. Al-Muhtaseb, *et al.*, Optimizing biodiesel production from waste with computational chemistry, machine learning and policy insights: a review, *Environ. Chem. Lett.*, 2024, **22**, 1005–1071, DOI: 10.1007/S10311-024-01700-Y.

92 PyTorch 2.4 Release Blog – PyTorch n.d. https://pytorch.org/blog/pytorch2-4/, accessed February 7, 2026.

93 M. W. Mumtaz, A. Adnan, Z. Mahmood, H. Mukhtar, M. F. Malik, F. A. Qureshi, *et al.*, Biodiesel from waste cooking oil: Optimization of production and monitoring of exhaust emission levels from its combustion in a diesel engine, *Int. J. Green Energy*, 2012, **9**, 685–701, DOI: 10.1080/15435075.2011.625583.

94 R. Jayabal, G. M. Lionus Leo, M. Chrispin Das, S. Sekar and S. Arivazhagan, Impact of ammonia energy fraction on improving thermal efficiency and emissions of ammonia/biodiesel in dual fuel diesel engine, *Process Saf. Environ. Prot.*, 2024, **188**, 1398–1410, DOI: 10.1016/J.PSEP.2024.06.016.

95 J. A. Caton, Combustion phasing for maximum efficiency for conventional and high efficiency engines, *Energy Convers. Manag.*, 2014, **77**, 564–576, DOI: 10.1016/j.enconman.2013.09.060.

96 A. Tarafdar, P. Majumder, M. Deb and U. K. Bera, Performance-emission optimization in a single cylinder CI-engine with diesel hydrogen dual fuel: A spherical fuzzy MARCOS MCGDM based Type-3 fuzzy logic approach, *Int. J. Hydrogen Energy*, 2023, **48**, 28601–28627, DOI: 10.1016/j.ijhydene.2023.04.019.

97 M. Ahmadi, D. Biswas, M. Lin, F. D. Vrionis, J. Hashemi and Y. Tang, Physics-informed machine learning for advancing computational medical imaging: integrating data-driven approaches with fundamental physical principles, *Artif. Intell. Rev.*, 2025, **58**, 297, DOI: 10.1007/S10462-025-11303-W.

98 K. Luo, S. Liao, Z. Guan and B. Liu, An enhanced hybrid adaptive physics-informed neural network for forward and inverse PDE problems, *Appl. Intell.*, 2025, **55**, 255, DOI: 10.1007/S10489-024-06195-2.

99 A. Latrach, M. L. Malki, M. Morales, M. Mehana and M. Rabiei, A critical review of physics-informed machine learning applications in subsurface energy systems, *Geoenergy Sci. Eng.*, 2024, **239**, 212938, DOI: 10.1016/j.geoen.2024.212938.

100 M. Z. Naser, Intuitive tests to validate machine learning models against physics and domain knowledge, *Digital Engineering*, 2025, **7**, 100057, DOI: 10.1016/j.dte.2025.100057.

101 C. Meng, S. Griesemer, D. Cao, S. Seo, Y. Liu. When physics meets machine learning: a survey of physics-informed machine learning. *Machine Learning for Computational Science and Engineering* 2025;1. doi: DOI: 10.1007/S44379-025-00016-0.

102 S. Ji, X. Li, W. Sun, H. Dong, A. Taalas, Y. Zhang, *et al.*, A Unified Review of Deep Learning for Automated Medical Coding, *ACM Comput. Surv.*, 2024, **56**, 1–41, DOI: 10.1145/3664615.

103 R. Mohan, T. Elsken, A. Zela, J. H. Metzen, B. Staffler, T. Brox, *et al.*, Neural Architecture Search for Dense Prediction Tasks in Computer Vision, *Int. J. Comput. Vis.*, 2023, **131**, 1784–1807, DOI: 10.1007/s11263-023-01785-y.

104 M. Lee, Mathematical Analysis and Performance Evaluation of the GELU Activation Function in Deep Learning, *J. Math.*, 2023, **2023**, 1–13, DOI: 10.1155/2023/4229924.

105 A. Wan, H. Zhang, T. Chen, K. AL-Bukhaiti and W. Wang, A hybrid deep learning model for robust aeroengine remaining useful life prediction. Signal, *Int. J. Video Image Process. Netw. Secur.*, 2025, **19**(7), 550, DOI: 10.1007/s11760-025-04150-3.

106 C. E. Üstün, R. D. S. M. De Freitas, E. C. Okafor, M. Shahbakhti, X. Jiang and A. Paykani, Machine Learning Applications for Predicting Fuel Ignition and Flame Properties: Current Status and Future Perspectives, *Energy Fuels*, 2025, **39**, 13281–13314, DOI: 10.1021/acs.energyfuels.5c02343.

107 A. Wan, S. Peng, K. AL-Bukhaiti, Y. Ji and S. Ma, The early warning method for offshore wind turbine gearbox oil temperature based on FSTAE-ATT, *Sustain. Comput.: Inform. Syst.*, 2025, **47**, 101180, DOI: 10.1016/j.suscom.2025.101180.

108 H. Girmay, K. Yeneneh and R. Gopal, Comprehensive analysis and prediction of biogas-diesel dual-fuel combustion in direct injection diesel engines: Experimental and artificial neural network approach, *Results Eng.*, 2025, **28**, 107773, DOI: 10.1016/j.rineng.2025.107773.

109 M. A. Modi, T. M. Patel. Optimizing Brake-Specific Energy Consumption in a Single-Cylinder Diesel Engine Fueled with Diesel and Polymer-Based Fuels. *Lecture Notes in Mechanical Engineering* 2026:295–312. doi: DOI: 10.1007/978-981-96-8508-0_24.

110 S. Vadlamudi, J. K. Panda, R. Rajan, K. Rajesh and S. P. Samal, Hydrogen–ammonia fuel blends for diesel engine performance, emissions, vibration–acoustic dynamics, and GEP optimization, *Environ. Prog. Sustain. Energy*, 2025, e70270, DOI: 10.1002/ep.70270.

111 A. Wan, S. Peng, K. AL-Bukhaiti, Y. Ji and S. Ma, The early warning method for offshore wind turbine gearbox oil temperature based on FSTAE-ATT, *Sustain. Comput.: Inform. Syst.*, 2025, **47**, 101180, DOI: 10.1016/j.suscom.2025.101180.

112 X. Li, Z. Wang, Y. Zhang, W. Zhang, H. Zhang, P. Liu and T. Lei, Hydrogen-rich gas formation from catalytic pyrolysis of biomass tar by aluminum dross coupled

HZSM-5 co-loaded Ni-Fe bimetallic catalysts: Influence of co-carrier characteristics, *J. Environ. Manage.*, 2025, **389**, 126016, DOI: 10.1016/j.jenvman.2025.126016.

113 A. K. Kausik, A. B. Rashid, R. F. Baki and M. M. Jannat Maktum, Machine learning algorithms for manufacturing quality assurance: A systematic review of performance metrics and applications, *Array*, 2025, **26**, 100393, DOI: 10.1016/j.array.2025.100393.

114 S. Rajendran, E. P. Venkatesan, R. Dhairiyasamy, S. Jaganathan, G. Muniyappan and N. Hasan, Enhancing Performance and Emission Characteristics of Biodiesel-Operated Compression Ignition Engines through Low Heat Rejection Mode and Antioxidant Additives: A Review, *ACS Omega*, 2023, **8**, 34281–34298, DOI: 10.1021/ACSOMEGA.3C03252.

115 D. Balasubramanian, T. Wongwuttanasatian, I. P. Venugopal and A. Rajarajan, Exploration of combustion behavior in a compression ignition engine fuelled with low-viscous Pimpinella anisum and waste cooking oil biodiesel blends, *J. Clean. Prod.*, 2022, **331**, 129999, DOI: 10.1016/j.jclepro.2021.129999.

116 G. Ramakrishnan, P. Krishnan, S. Rathinam, R. Thiyagu and Y. Devarajan, Role of nano-additive blended biodiesel on emission characteristics of the research diesel engine, *Int. J. Green Energy*, 2019, **16**, 435–441, DOI: 10.1080/15435075.2019.1577742.

117 R. Jayabal, Environmental impact of adding hybrid nanoparticles and hydrogen to the algae biodiesel-diesel blend on engine emissions, *Process Saf. Environ. Prot.*, 2025, **198**, 107102, DOI: 10.1016/j.psep.2025.107102.

118 G. Dhamodaran, S. Venugopal, S. Seetharaman and T. Palsami, Comparative analysis of a diesel engine fueled with hydrogen-enriched nanoparticle-emulsified second-generation biodiesel, *Fuel*, 2026, **409**, 137851, DOI: 10.1016/j.fuel.2025.137851.

119 F. Polat, S. Sarıdemir, M. S. Gad, A. S. El-Shafay and Ü. Ağbulut, Enhancing diesel engine performance, combustion, and emissions reductions under the effect of cerium oxide nanoparticles with hydrogen addition to biodiesel fuel, *Int. J. Hydrogen Energy*, 2024, **83**, 884–896, DOI: 10.1016/j.ijhydene.2024.08.031.

120 S. Talesh Amiri, R. Shafaghat, O. Jahanian and R. Alamian, Experimental study on high fatty acid WCO biodiesel effects on RCCI engine performance, and emissions, considering fuel oxygen level, *Biofuels*, 2025, **16**, 697–705, DOI: 10.1080/17597269.2025.2450167.

121 E. Sangeethkumar, M. Jaikumar, P. Vijayabalan, H. A. Mahmood, A. O. Al-Sulttani, *et al.*, The effect of using the WCO biodiesel as an alternative fuel in compression ignition diesel engine on performance and emissions characteristics, *J. Phys., Conf. Ser.*, 2022, **2299**, 012023, DOI: 10.1088/1742-6596/2299/1/012023.

122 S. Li, Q. Yang, L. Ye, H. Du, Z. Zhang, X. Huang, *et al.*, Effect of Nanoparticle Concentration on Physical and Heat-Transfer Properties and Evaporation Characteristics of Graphite/n-Decane Nanofluid Fuels, *ACS Omega*, 2022, **7**, 3284–3292, DOI: 10.1021/ACSOMEGA.1C05343.

123 Y. C. Hsiao, Y. Deng and S. L. Lin, Enhanced performance and reduced emissions of regulated pollutants and (nitrated) polycyclic aromatic hydrocarbons using CeO2 and CuO–CeO2 nanoparticle diesel additives, *Next Energy*, 2025, **9**, 100454, DOI: 10.1016/j.nxener.2025.100454.

124 J. S. Basha, B. M. Al, M. E. M. Soudagar, M. R. Safaei, M. A. Mujtaba, T. M. Y. Khan, *et al.*, Applications of Nano-Additives in Internal Combustion Engines: A Critical Review, *J. Therm. Anal. Calorim.*, 2022, **147**, 9383–9403, DOI: 10.1007/S10973-022-11199-6.

125 Y. Singh, H. S. Pali, N. K. Singh, A. Sharma and A. Singla, Effect of nanoparticles as additives to the biofuels and their feasibility assessment on the engine performance and emission analysis—A review, *Proc. Inst. Mech. Eng. Part E J. Process Mech. Eng.*, 2023, **237**, 492–510, DOI: 10.1177/09544089221109723.

126 K. B. Sasidhar, M. Somasundaram, K. Yesuraj, S. Hariharan, E. Antunes, P. Ekambaram, *et al.*, Optimization and production of renewable fuels from waste cooking oil and low-density polyethylene: Evaluating fuel properties and techno-economic feasibility of diesel replacement, *Energy Convers. Manag.*, 2023, **294**, 117558, DOI: 10.1016/j.enconman.2023.117558.

127 B. Çiftçi, M. Karagöz, M. Aydin and M. B. Çelik, The effect of fusel oil and waste biodiesel fuel blends on a CI engine performance, emissions, and combustion characteristics, *J. Therm. Anal. Calorim.*, 2024, **149**, 7783–7796, DOI: 10.1007/S10973-024-13285-3.

128 M. Deka, P. K. Mahanta, N. D. Choudhury. Effect of EGR on Performance and Emission Characteristics of a Diesel Engine Fueled with Yellow Oleander Seed Oil Biodiesel. *Lecture Notes in Mechanical Engineering* 2022:351–363. doi: DOI: 10.1007/978-981-16-3497-0_27.

129 M. Noman, M. Farooq, A. Ramli, D. Muhammad, F. Perveen, J. Sahar, *et al.*, Optimizing acid heterogeneous catalyzed biodiesel production from diverse feedstocks: A sustainable approach to renewable energy, *Chem. Eng. Res. Des.*, 2025, **220**, 500–513, DOI: 10.1016/j.cherd.2025.07.029.

130 M. Mofijur, S. F. Ahmed, B. Ahmed, T. Mehnaz, F. Mehejabin, S. Shome, *et al.*, Impact of nanoparticle-based fuel additives on biodiesel combustion: An analysis of fuel properties, engine performance, emissions, and combustion characteristics, *Energy Convers. Manag.*, 2024, **21**, 100515, DOI: 10.1016/j.ecmx.2023.100515.

131 S. Xu, Z. Tian and H. Liu, Development of a Skeletal Mechanism with NOx Chemistry for CH4/H2 Combustion over a Wide Range of Hydrogen-Blending Ratios, *Energy Fuels*, 2024, **38**, 19758–19777, DOI: 10.1021/ACS.ENERGYFUELS.4C02802.

132 G. M. L. Leo, S. Sekar and S. Arivazhagan, Experimental investigation and ANN modelling of the effects of diesel/gasoline premixing in a waste cooking oil-fuelled HCCI-DI engine, *J. Therm. Anal. Calorim.*, 2020, **141**, 2311–2324, DOI: 10.1007/S10973-020-09418-Z.

133 G. M. Lionus Leo, S. Sekar and S. Arivazhagan, Experimental investigation, optimization and ANN model

prediction of a gasoline premixed waste cooking oil fueled HCCI–DI engine, *J. Braz. Soc. Mech. Sci. Eng.*, 2018, **40**, 1–14, DOI: 10.1007/S40430-018-0967-1/TABLES/8.

134 S. Muniyappan and R. Krishnaiah, Investigation on the Effects of the ZnO Combustion Enhancer to Ascertain the Blend Ratio Using Artificial Intelligence and a Statistical Approach for a Diesel-Biodiesel-Ethanol-Fueled CI Engine, *ACS Omega*, 2025, **10**, 26579–26604, DOI: 10.1021/ACSOMEGA.5C00624.

135 G. M. Lionus Leo, A. Sundaraganesan and S. Subramani, Experimental investigation, ANN modelling and TOPSIS optimization of a gasoline premixed HCCI-DI engine with direct injection of FeCl3 nanoadditive blended WCO, *Trans. FAMENA*, 2019, **43**, 83–100, DOI: 10.21278/TOF.43306.

136 L. E. O. G. Lionus, S. Sekar, G. Ashwin PRABHU and P. Prabhakar, Optimizing Thermal Efficiency and Emissions in Hybrid HCCI-DI Combustion with Biodiesel-Diethyl Ether-Nanoparticle Blends Biyodizel-Dietil Eter-Nanoparçacık Karışımları ile Hibrit HCCI-DI Yanmasında Termal Verimlilik ve Emisyonların Optimizasyonu, *J. Therm. Sci. Technol.*, 2025, **45**, 193–206, DOI: 10.47480/isibted.1630463.

137 G. M. Lionus Leo, R. Jayabal, D. Srinivasan, M. Chrispin Das, M. Ganesh and T. Gavaskar, Predicting the performance and emissions of an HCCI-DI engine powered by waste cooking oil biodiesel with Al2O3 and FeCl3 nano additives and gasoline injection – A random forest machine learning approach, *Fuel*, 2024, **357**, 129914, DOI: 10.1016/j.fuel.2023.129914.

138 G. M. Lionus Leo, R. Jayabal, D. Srinivasan, M. Chrispin Das, M. Ganesh and T. Gavaskar, Predicting the performance and emissions of an HCCI-DI engine powered by waste cooking oil biodiesel with Al2O3 and FeCl3 nano additives and gasoline injection – A random forest machine learning approach, *Fuel*, 2024, **357**, 129914, DOI: 10.1016/J.FUEL.2023.129914.

139 S. Guo, J. Wang, W. Zhang, M. Zhang and Z. Huang, Effect of hydrogen enrichment on swirl/bluff-body lean premixed flame stabilization, *Int. J. Hydrogen Energy*, 2020, **45**, 10906–10919, DOI: 10.1016/j.ijhydene.2020.02.020.

140 E. Ramachandran, R. Krishnaiah, E. Perumal Venkatesan, S. R. Medapati, R. Sabarish, S. A. Khan, *et al.*, Experimental Studies to Reduce Usage of Fossil Fuels and Improve Green Fuels by Adopting Hydrogen-Ammonia-Biodiesel as Trinary Fuel for RCCI Engine, *ACS Omega*, 2024, **9**, 741–752, DOI: 10.1021/acsomega.3c06327.

141 J. Li, Z. Zhao, A. Kazakov, M. Chaos, F. L. Dryer and J. I. Scire, A comprehensive kinetic mechanism for CO, CH2O, and CH 3OH combustion, *Int. J. Chem. Kinet.*, 2007, **39**, 109–136, DOI: 10.1002/kin.20218.

142 S. Li, Q. Yang, L. Ye, H. Du, Z. Zhang, X. Huang, *et al.*, Effect of Nanoparticle Concentration on Physical and Heat-Transfer Properties and Evaporation Characteristics of Graphite/n-Decane Nanofluid Fuels, *ACS Omega*, 2022, **7**, 3284–3292, DOI: 10.1021/acsomega.1c05343.

143 J. Liu, C. Ulishney and C. E. Dumitrescu, Random forest machine learning model for predicting combustion feedback information of a natural gas spark ignition engine, *J. Energy Resour. Technol.*, 2021, **143**, 012301, DOI: 10.1115/1.4047761.

144 S. Kesharvani, S. Katre, S. Pandey, G. Dwivedi, T. N. Verma and P. Baredar, Optimizing Biodiesel Production from Karanja and Algae Oil with Nano Catalyst: RSM and ANN Approach, *Energy Eng. J. Assoc. Energy Eng.*, 2024, **121**, 2363–2388, DOI: 10.32604/ee.2024.052523.

145 A. Natarajan, A. Kandasamy, E. Perumal Venkatesan and C. A. Saleel, Experimental Investigation on the Effect of Graphene Oxide in Higher Alcohol Blends and Optimization of Injection Timing Using an ANN Method, *ACS Omega*, 2023, **8**, 41339–41355, DOI: 10.1021/ACSOMEGA.3C04895.

146 R. Matai, Surrogate modeling for flow simulations using design variable-coded deep learning networks, *J. Eng. Appl. Sci.*, 2025, **72**(1), DOI: 10.1186/S44147-025-00634-8.

147 B. Sun, L. Ma, T. Shen, R. Geng, Y. Zhou and Y. Tian, A robust data-driven method for multiseasonality and heteroscedasticity in time series preprocessing, *Int. J. Comput. Netw. Wirel. Mob. Commun. (IJCNWMC)*, 2021, **2021**, 6692390, DOI: 10.1155/2021/6692390.

148 S. Tripathi, D. Muhr, M. Brunner, H. Jodlbauer, M. Dehmer and F. Emmert-Streib, Ensuring the Robustness and Reliability of Data-Driven Knowledge Discovery Models in Production and Manufacturing, *Front. Artif. Intell.*, 2021, **4**, 576892, DOI: 10.3389/frai.2021.576892.

149 W. Zeng, J. Fu, F. Zhou, J. Yu, J. Liu and K. Yuan, Prediction of transient NOX emission from a non-road diesel engine using a model combining Bayesian search and Population-based training, *Atmos. Environ.*, 2024, **321**, 120350, DOI: 10.1016/j.atmosenv.2024.120350.

150 S. Yongqiang, Z. Lvfang, S. Yaozhang and W. Lili, Research on the enhancement method of offshore vessel characteristics based on transplanting memory LSTM, *Mar. Geod.*, 2026, 1–32, DOI: 10.1080/01490419.2025.2612187.

151 O. Fink, V. Sharma, I. Nejjar, L. Von Krannichfeldt, S. Garmaev, Z. Zhang, *et al.*, From physics to machine learning and back: Part I - Learning with inductive biases in prognostics and health management (PHM), *Reliab. Eng. Syst. Saf.*, 2026, **271**, 112213, DOI: 10.1016/j.ress.2026.112213.

152 A. M. Ansari, F. A. Solangi, A. N. Sanjrani, F. Hussain, B. Zhang, Z. Ding, *et al.*, Enhancing Engine Reliability with Machine Learning Techniques on Spark Plug Deposition using Green Alcohol Blend Fuels on Gasoline Engine, *Results Eng.*, 2026, 108975, DOI: 10.1016/j.rineng.2026.108975.

153 M. R. Santos, A. Guedes and I. Sanchez-Gendriz, SHapley Additive exPlanations (SHAP) for Efficient Feature Selection in Rolling Bearing Fault Diagnosis, *Machine Learning and Knowledge Extraction*, 2024, (6), 316–341, DOI: 10.3390/make6010016.

154 J. P. Szybist, S. Busch, R. L. McCormick, J. A. Pihl, D. A. Splitter, M. A. Ratcliff, *et al.*, What fuel properties enable higher thermal efficiency in spark-ignited engines?, *Prog. Energy Combust. Sci.*, 2021, **82**, 100876, DOI: 10.1016/j.pecs.2020.100876.

155 Y. JIA, Y. LIU, X. HE, Z. MENG and S. ZHAO, Arrangement guideline of film holes along conjugate temperature difference in turbine guide vanes, *Chin. J. Aeronaut.*, 2025, **38**(6), 103400, DOI: 10.1016/j.cja.2025.103400.

156 R. Kumar, M. Yadav, A. Rana, B. Singh, Y. S. Meena, D. Tripathi, *et al.*, Heterogeneous Bismuth Nanocatalyst for Selective Hydrogenation of Alkenes, *ACS Appl. Nano Mater.*, 2025, **8**, 3436–3449, DOI: 10.1021/acsanm.4c06452.

157 P. Kumar and A. K. Pal, Study on the performance and emissions characteristics of reformulated engine blended with producer gas, biogas, and pongamia pinnata biodiesel, *Next Sustain.*, 2025, **5**, 100138, DOI: 10.1016/j.nxsust.2025.100138.

158 S. D. Jadhav and M. S. Tandale, Part load and full load multi-objective performance optimization of a single-cylinder diesel engine operating on Mangifera indica biodiesel as biofuel, *Biofuels*, 2018, **9**, 29–44, DOI: 10.1080/17597269.2016.1249740.